2011
2012

GENEESKUNDE

master in de biomedische wetenschappen: klinische moleculaire wetenschappen

Masterproef

The influence of aquaporin-4 isoform interaction on supramolecular water channel assembly in astrocytoma cells

Promotor :
Prof. dr. Rafael DE JONGH
Prof. dr. Marcel AMELOOT

Sarah Deville

Masterproef voorgedragen tot het bekomen van de graad van master in de biomedische wetenschappen , afstudeerrichting klinische moleculaire wetenschappen

Maastricht University

universiteit hasselt
KNOWLEDGE IN ACTION

De transnationale Universiteit Limburg is een uniek samenwerkingsverband van twee universiteiten in twee landen: de Universiteit Hasselt en Maastricht University

universiteit hasselt
KNOWLEDGE IN ACTION

Maastricht University

Universiteit Hasselt | Campus Diepenbeek | Agoralaan Gebouw D | BE-3590 Diepenbeek
Universiteit Hasselt | Campus Hasselt | Martelarenlaan 42 | BE-3500 Hasselt

2011
2012

GENEESKUNDE

master in de biomedische wetenschappen: klinische moleculaire wetenschappen

Masterproef

The influence of aquaporin-4 isoform interaction on supramolecular water channel assembly in astrocytoma cells

Promotor :
Prof. dr. Rafael DE JONGH
Prof. dr. Marcel AMELOOT

Sarah Deville

Masterproef voorgedragen tot het bekomen van de graad van master in de biomedische wetenschappen , afstudeerrichting klinische moleculaire wetenschappen

Maastricht University

universiteit hasselt
KNOWLEDGE IN ACTION

Table of contents

List of abbreviations

A	Degree of aggregation
ANOVA	Analysis of variance
AQP	Aquaporin
BBB	Blood brain barrier
BP	Band-pass filter
BSA	Bovine serum albumin
CamKII	Calcium-calmodulin-dependent kinase II
CKII	Casein kinase II
CLSM	Confocal laser scanner microscope
CNS	Central nervous system
DMD	Dystrophin
DMEM	Dulbecco's modified eagle's medium
FCS	Fluorescence correlation spectroscopy
FFEM	Freeze fracture electron microscopy
FRAP	Fluorescence recovery after photobleaching
HA	Human astrocytoma 132N1 cells
HFT	Main dichroic beam splitter
HR	Histamine receptor
ICP	Intracranial pressure
ICS	Image correlation spectroscopy
KP	Short-pass filter
MSD	Mean square displacement
MWPR	DMEM without phenol red
NFT	Secondary dichroic beam splitter
OAP	Orthogonal array of particles
ρ	Particle density
PBS	Phosphate buffered saline
PFA	Paraformaldehyde
PKA	Protein kinase A
PKC	Protein kinase C
PKG	Protein kinase G
PMT	Photomultiplier tube
ROI	Region of interest
SEM	Standard error of the mean
SNTA	α-syntrophin
SPT	Single particle tracking
TBI	Traumatic brain injury
TICS	Temporal image correlation spectroscopy
TIRF	Total internal reflection fluorescence

Acknowledgements

This master thesis would not have been possible without the guidance and the support of several persons who contributed and extended their valuable assistance in the preparation and completion of this study.

First of all, I would like to thank Prof. Dr. Raf De Jongh, my promoter, for giving me the chance to perform my senior internship on this project. Furthermore, I am grateful to Prof. Dr. Marcel Ameloot for giving me the opportunity to perform my senior internship at the Biomedical Research Institute at the division of Biophysics. Moreover, a special thank for Dr. Rony Nuydens for his support during my internship. In addition, I would like to thank you all for your suggestions and your critical view on my master thesis.

I would like to thank Prof. Dr. Niels Hellings, my second examiner, for his suggestions and for his help during this project.

I want to express gratitude to Kristof Notelaers, my supervisor, for his support in a number of ways. I would like to thank you for your help in the lab, your assistance at the confocal microscope and for your suggestions for my master thesis. As well, I would like to thank you and Dr. Nick Smisdom for the assistance with the data analyses. Additionally, I would like to thank all the members of Biophysics - Mihaela Bacalum, Ben De Clercq, Rik Paesen and Kathleen Sanen - for their support and guidance during my internship.

I would also like to show gratitude to Anke Smets and Ingrid Meex for their help during my internship and the completion of my master thesis. Likewise, I would like to thank Jo Janssen for his assistance in the cell culture lab.

I am indebted to my many of my student colleagues to support me during this period.

To close, special thanks to my family for giving me the chance to complete this master education program and for their unconditional support during this master thesis.

Sarah Deville,
11th June 2012.

Abstract

Traumatic brain injury (TBI) is a leading cause of death and disability worldwide. TBI is often complicated by the development of brain edema. Despite its clinical importance, the underlying pathological mechanisms are poorly understood. Nevertheless, a central role for aquaporin-4 (AQP4) has been suggested. AQP4 is the predominant water channel of the central nervous system (CNS) which plays a key role in maintaining the water homeostasis in the brain. The isoform ratio of AQP4-M1 and AQP4-M23 is deterministic for assembly in supramolecular structures named orthogonal arrays of particles (OAP), which are essential for channel opening. It has been postulated that AQP4 can be dynamically regulated by numerous stimuli, both in physiological and pathological conditions, allowing the cell to rapidly adjust their water permeability. Dissociation of OAP or their dramatic reduction after TBI has a serious impact on the pathological response of the CNS, where both water accumulation and clearance are dramatically compromised. In present study, it was hypothesized that the neuronal mediator histamine, which is extensively released following TBI, disrupts the astrocytic AQP4 supramolecular organization in OAP. In order to address questions about the regulation of OAP dynamics and membrane organization, the clustering in OAP should be accurately determined. For that reason, the dynamic behavior of AQP4-M1 and AQP4-M23 in the cell membrane of astrocytoma cells was investigated by microfluorimetric techniques including immunofluorescence, image correlation spectroscopy (ICS), fluorescence recovery after photobleaching (FRAP) and single particle tracking (SPT). Thereafter, the effect of histamine on OAP in AQP4 expressing cells was explored using aforementioned techniques. ICS generated more insights in the aggregation of AQP4 in OAP. FRAP revealed that AQP4-M1 freely circulated in membranes whereas AQP4-M23 was nearly immobile. FRAP was not feasible in studying the OAP formation as the movement of AQP4-M23 clusters in and out the bleach region dramatically affected the recovery curve. SPT was used instead to investigate AQP4-M23 motions. Exposure to histamine induced a rapid decrease of membrane-associated AQP4 with an accumulation of AQP4 containing vesicles inside the cell. ICS showed that this internalization was accompanied with a decreased OAP size. Furthermore, this was in agreement an increased mobility of AQP4-M1 and AQP4-M23. In present study, a negative correlation between histamine and AQP4 was found. Loss of water channels may impair the rate of water flow in the brain and thereby affecting the course of TBI as well. Microfluorimetric measurements proved to be a significant tool in studying OAP formation quantitatively in living cells. The obtained biophysical data opens opportunities to elucidate the mechanisms involved in OAP regulation.

Samenvatting

Een traumatisch hersenletsel (TBI) is wereldwijd een belangrijke oorzaak van sterfte en blijvende neurologische schade. Vaak wordt TBI gecompliceerd door de ontwikkeling van hersenoedeem. Ondanks het klinische belang zijn de onderliggende pathologische mechanismen slechts weinig gekend. Desondanks wordt aquaporine-4 (AQP4) gesuggereerd een centrale rol te spelen. AQP4 is het predominante waterkanaal van het centrale zenuwstelsel (CZS) waarbij het betrokken is in het behouden van de waterhomeostase in de hersenen. De ratio van twee belangrijke AQP4 isovormen, AQP4-M1 en AQP4-M23, is bepalend voor de formatie van supramoleculaire structuren, de zogenaamde *orthogonal arrays of particles* (OAP). De organisatie in OAP is essentieel voor waterkanaal opening. AQP4 wordt beoogd om dynamisch gereguleerd te worden onder zowel fysiologische als pathologische condities. Dit laat een cel toe om snel zijn waterpermeabiliteit aan te passen. Dissociatie of reductie van OAP na TBI heeft serieuze impact op de pathologische respons van het CZS, waarbij zowel de wateraccumulatie als de klaring ervan verstoord worden. In deze studie werd onderzocht of de neuronale mediator histamine, welke veelvoudig vrijgezet wordt na TBI, de astrocytische AQP4 organisatie in OAP verstoord. Om AQP4 organisatie en dynamische regulatie van OAP verder te bestuderen, moet de clustering in OAP accuraat bepaald worden. Om deze reden, werd het dynamisch gedrag van AQP4-M1 en AQP4-M23 in het celmembraan van astrocytomacellen onderzocht met behulp van microfluorimetrische technieken, meer bepaald immunofluorescentie, *image correlation spectroscopy* (ICS), *fluorescence recovery after photobleaching* (FRAP) en *single particle tracking* (SPT). Hierna werd het effect van histamine op de OAP van AQP4 onderzocht gebruik makend van bovenstaande technieken. Meer inzichten over de aggregatie van AQP4 in OAP werd vergaard door middel van ICS. FRAP toonde aan dat AQP4-M1 vrij diffundeerde in het celmembraan, waarbij AQP4-M23 bijna immobiel was. FRAP was niet toepasbaar in het bestuderen van OAP formatie omdat de beweging van AQP4-M23 clusters in en uit de bleekregio interfereerde met het herstel van het fluorescentiesignaal. In plaats hiervan werd SPT gebruikt om de diffusie van deze isovorm te bestuderen. Blootstelling aan histamine induceerde een snelle vermindering in het membraan-geassocieerde AQP4 samengaand met een intracellulaire accumulatie van met AQP4 gevulde vesikels. ICS toonde aan dat deze internalisatie samenging met een verminderde OAP grootte. Dit was in overeenkomst met een verhoogde diffusie van AQP4-M1 and AQP4-M23. Samenvattend werd in deze studie negatieve correlatie gevonden tussen histamine en AQP4. Verlies van waterkanalen kan de waterstroom in de hersenen verstoren en bijgevolg het klinisch verloop van TBI beïnvoeden. Bovendien toont deze studie het belang aan van microfluorimetrische metingen voor het onderzoeken van OAP formatie. De bekomen biofysische data opent mogelijkheden om de mechanismen betrokken in de regulatie van OAP verder te bestuderen.

Chapter 1: Introduction

Traumatic brain injury (TBI) is a leading cause of death and disability worldwide. It is the most common cause of death in the developed world in those aged below 40 years (1). The development of brain edema following TBI causes brain swelling and increased intracranial pressure (ICP), which may result in secondary neuronal damage, brain herniation and eventually death. Despite its clinical importance, current therapeutic strategies only provide a symptomatic relief without addressing the underlying pathological mechanisms (2). The cellular and molecular mechanisms contributing to the development or resolution of TBI-associated brain edema are poorly understood. Nevertheless, recent data suggests a central role for the aquaporin water channels (AQP) in keeping water homeostasis in the brain. Aquaporin-4 (AQP4), the predominant water channel of the central nervous system (CNS), has demonstrated to be involved in both the development and resolution of brain edema (1).

1.1 AQP water channel family

AQPs are small hydrophobic, integral membrane proteins found in organisms from all kingdoms of life, including unicellular organisms such as bacteria and yeasts and multicellular organisms such as plants, animals and humans (3). To date, thirteen human AQPs – named AQP0-12 – have been identified. A typical AQP water channel contains six membrane-spanning α-helices, with both the N- and C- terminus located on the cytoplasmic side of the membrane (4). The two halves of the protein have an obvious structural symmetry; with each halve dipping into the middle of the lipid bilayer to form two hemipores that together create a pore, which facilitates an osmotically driven bidirectional water flow. The selectivity for the passage of water is due to electrostatic forces within the pore, causing water molecules to flip. Breaking the interaction with charged molecules within the pore, enables the translocation of the water molecules (5). Based on their permeability characteristics, AQPs are classified in two main groups. The orthodox AQPs including AQP1, AQP2, AQP4, AQP5, AQP6 and AQP8; which are only permeable to water, whereas the aquaglyceroporines including AQP3, AQP7, AQP9 and AQP10, also allow the transport of small and uncharged solutes such as glycerol and urea (4). The permeability properties of AQP0, 11 and 12 are still ambiguous (6). At structural level, AQPs usually form tetramers where the tetrameric assembly is crucial for the proper folding, stability, targeting to the plasma membrane and even the functionality of the water channel. Although each monomer provides its own functional water pore, the properties of this pore are determined by cooperative interaction of the entire tetramer (5).

1.2 AQP4

AQP4 is, as mentioned before, by far the most abundant water channel protein in the central nervous system (CNS). Here, AQP4 is predominantly expressed by astrocytes and ependymal cells whereas neurons, oligodendrocytes and resting microglia are devoid of AQP4 (7). In astrocytes, the characteristic subcellular distribution of AQP4 is a basic property in which the AQP4 expression is enriched in the perivascular astrocyte endfeet, in perisynaptic astrocyte processes and in the processes that are in contact with the nodes of Ranvier and nonmyelinated axons (8). This

localized distribution suggests that AQP4 contributes in facilitating the bidirectional water flow across the blood-brain interfaces (9). At the molecular level, AQP4 exists in two major isoforms due to the two different translation initiation sites at methionine 1, or at methionine 23. This altered translation results in a 323 amino acid AQP4-M1 or a 301 amino acid AQP4-M23 isoform **(figure 1A)** (7, 10). According to other AQPs, AQP4 molecules assemble in homotetramers or heterotetramers where each tetramer contains four functional water channels. Furthermore, these tetramers can form supramolecular structures named orthogonal arrays of particles (OAP) visualized as square arrays of particles by freeze-fracture electron microscopy (FFEM) **(figure 1B-C)** (10). The functional importance of supramolecular water channel assembly is that the higher-order organization in OAPs increases single-channel osmotic water permeability by one order of magnitude (11). Quantitative cellular expression of AQP4 isoforms regulates this organization (12). AQP4-M1 is responsible for downregulating the OAP size, whereas AQP4-M23 favors OAP assembly. OAP formation is mediated by two symmetric interactions between arginine 108 of each molecule and tyrosine 250 of another molecule in the neighboring tetramer. This interaction is prevented in the AQP4-M1 since arginine 9 at the N-terminus, which is absent in the AQP4-M23, forms an intramolecular bond with tyrosine 250 (13). OAP formation can be regulated by the modification of intracellular cysteine residues of AQP4-M1 by palmitoylation (9). These extra residues block tetramer-tetramer contacts between adjacent AQP4-M23 termini. This reversible modification is highly regulated, but little is known about the mechanisms controlling this process (14). Regulation of the astrocyte OAPs might facilitate AQP4 water transport, cellular polarization and cell-cell adhesion (6, 12).

The extent of transmembrane water transport through AQP4 is principally dependent on the single channel water permeability, the abundance of channels present in the plasma membrane and the difference in osmotic pressure between both sides of the membrane (7). AQP4 has multiple phosphorylation sites which are involved in the dynamic regulation of AQP4 (15). Phosphorylation by protein kinases such as protein kinase C (PKC), protein kinase A (PKA), calcium-calmodulin-dependent kinase II (CamKII), casein kinase II (CKII) and protein kinase G (PKG) involve several processes including gating, protein internalization, lysosomal targeting and Golgi transition of AQP4 (16).

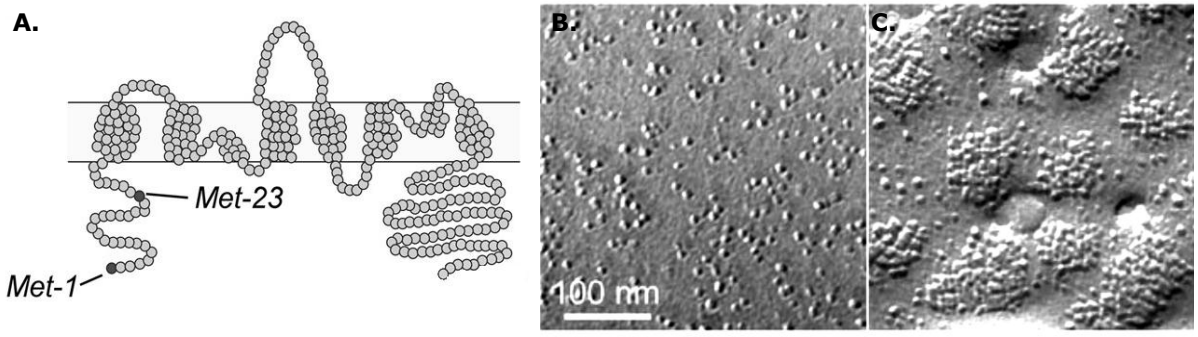

Figure 1: AQP4 structure and assembly in orthogonal arrays of particles. **(A)** Membrane topology of AQP4, comprising six bilayer-spanning domains and five connecting loops. At the N-terminus, the initiation sites at methionine 1 and 23 are shown, resulting in the AQP4-M1 and AQP4-M23 isoforms. **(B+C)** Freeze-fracture electron micrographs of the plasma membrane of COS-7 cells transfected with **(B)** AQP4-M1 or **(C)** AQP4-M23 (scale bar is 100 nm). The M1 tetramers are largely dispersed over the plasma membrane, whereas the M23 tetramers form large OAPs. *Adapted from Crane et al, 2008-2010 (10, 17).*

Activation of PKC leads to a rapid decline in water permeability, mediated by an allosteric alteration of AQP4 (18). PKA, CamKII, CKII and PKG have not been reported to influence the water permeability of AQP4, but their phosphorylation might provide a mechanism that regulates AQP4 cell surface expression, and thereby affecting overall water permeability of the plasma membrane (15). The rate of maximum water transport by AQP4 is predominantly influenced by the AQP4-M1 to AQP4-M23 expression ratio and its ratio-dependent assembly in OAPs and other substances that regulate AQP4 gating including PKC (7).

1.3 Traumatic brain injury and brain edema

In TBI, an alteration in brain function, or other evidence of brain pathology is caused by an external force (19). This force causes tissue distortion, shearing and destruction resulting in a primary injury. The clinical outcome is profoundly dependent on the ensuing biochemical and cellular events occurring minutes to weeks after the primary insult. The following secondary injury mechanisms comprise an extensive range of processes such as disturbance of the ionic homeostasis, glutamate excitotoxicity, free radical generation, lipid peroxidation, blood–brain barrier (BBB) disruption, secondary hemorrhage, ischemia, intracranial hypertension, inflammation and cell death (20). The release of neuronal mediators in above-mentioned processes contributes to the development of brain edema. This increased brain volume is the result from localized or diffuse fluid accumulation within the brain parenchyma. Initially, brain volume changes are compensated by a reduction in cerebrospinal fluid (CSF) and blood volume. However, failure of this compensatory mechanism results in the development of brain edema (21).

The association with either extra- of intracellular fluid accumulation leads to the classification into vasogenic and cytotoxic brain edema (22). In vasogenic brain edema, mechanical injury and destructive mediators contribute to an increased permeability of the BBB. The hydrostatic pressure gradient between blood and brain results in the entry of a protein-rich exudate into the brain (23). In contrast, cytotoxic brain edema – characterized by intracellular water accumulation in both astrocytes and neurons – occurs independently of the BBB integrity. Impaired regulation of the cerebral blood flow and metabolism results in depletion of ATP stores and failure of energy-dependent ion pumps. The inability of the cells to regulate their volume, results in a shift of water from the interstitial into the intracellular compartment (22, 23). Both vasogenic and cytotoxic brain edema present following TBI. Vasogenic brain edema is the most prevailing edema, though cytotoxic brain edema develops early and persist while BBB integrity is gradually restored (24). The clearance of edema fluid – in both vasogenic and cytotoxic edema – follows three different routes: (a) across the glia limitans into the CSF in the subarachnoid space; (b) across the BBB into the bloodstream and (c) across the ependymal cells into the ventricles **(figure 2)** (22). The strategic localization of AQP4 at these exit routes suggests a key role for AQP4 mediated water transport in brain edema (23).

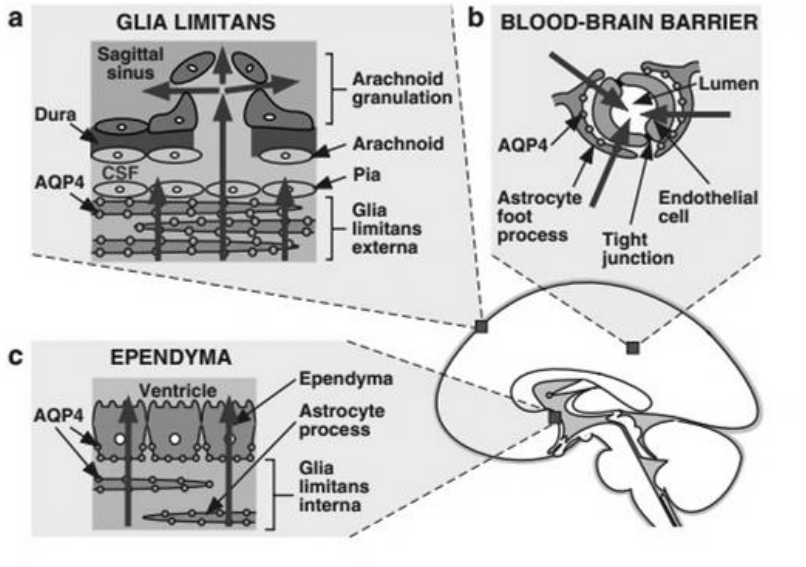

Figure 2: Routes of water exit from the brain in brain edema. In both cytotoxic and vasogenic types of brain edema, excess fluid is eliminated through aquaporin-4 (AQP4) rich barriers: **(A)** The glia limitans externa into the subarachnoid space; **(B)** the blood–brain barrier into the bloodstream; **(C)** the glia limitans interna and ependymal into the ventricles. *Adapted from Papadopoulos and Verkman, 2007 (22).*

1.4 A dual role for AQP4 in brain edema

The first evidence for AQP4 involvement in brain edema was provided by studies with AQP4-null mice. Loss of this protein significantly impacts the pathological response of the CNS (23). First, the effect of AQP4 deletion on cytotoxic brain edema was investigated using a model of water intoxication. Here, intraperitoneal water infusion causes serum hyponatremia, in turn creating an osmotic gradient driving water entry into the brain and causing cytotoxic edema. AQP4-null mice showed an improved survival and functional outcome compared to wild-type constraints (25). Furthermore, the effect of AQP4 deletion was studied in permanent middle cerebral artery occlusion, which is a clinically relevant model of stroke, resulting predominantly in cytotoxic brain edema. AQP4-null mice had a reduced mortality rate, diminished infarct volumes and less neurological deficits (25). Comparable effects of AQP4 deletion where observed in meningitis induced brain edema where AQP4-null mice had a remarkably lower ICP and brain water accumulation and an improved outcome (26).

AQP4 deletion impairs water entry into the brain and thereby limiting the edema formation. However, as AQP4 permits bidirectional water transport, AQP4 is not only a major pathway for water entry but also for water exit (27). Therefore, the role of AQP4 in brain water exit was further explored. After intracerebral fluid infusion, AQP4-null mice developed higher ICP and brain water content (28). Next, a focal cortical freeze injury model was employed as it is a highly reproducible model of vasogenic brain edema (27). It was shown that AQP4 deficiency resulted in a worse clinical outcome, higher ICP and a greater brain water content compared to controls (28). AQP4 deletion resulted in worsening of vasogenic edema due to an impaired clearance by a transcellular AQP4-dependent route (23).

After studies with AQP4-null mice, alternative approaches were used to test the function of this water channel. Anchoring of AQP4 to the astrocytic foot processes is dependent on the dystrophin (DMD) – α-syntrophin (SNTA) complex. DMD binds to dystrobrevin, which provides a scaffold for syntrophins including SNTA. AQP4 binds to the DMD-SNTA complex through interaction with SNTA (23). In SNTA deficient mice, the polarized pattern of AQP4 distribution is disrupted. Here, the development of cytotoxic brain edema was significantly retarded following hyponatremia and middle cerebral artery occlusion (8). The complete deficiency of DMD-SNTA complex in *dmx* mice, which carry a spontaneous mutation that prevents the expression of the largest isoform of DMD, had a similar impact, delaying cytotoxic brain edema after hyponatremia (29). As both mouse strains had similar AQP4 expression as the wild-type controls, mislocalization alone was sufficient to impair channel function to a significant extent (23).

These findings point out that an alteration in OAP structure may as well narrow down AQP4 mediated water transport (11). Dissociation of OAPs or their dramatic reduction has been observed in several neurological disease processes, including cerebral ischemia, aluminum-induced epilepsy and as an early event after a circulatory arrest (30). As AQP4 has a substantial impact on the pathological response of the CNS after these events, OAP loss might be a significant parameter influencing the outcome of the disease process. Decreased AQP4 function would diminish edema fluid elimination, but it would also slow down the formation of cytotoxic brain edema. Though, the mechanisms responsible for this OAP loss are not yet elucidated.

1.5 Histamine and AQP4

Histamine is a neurotransmitter and neuromodulator within the CNS. Histaminergic neurons are located in the tuberomamillary nuclei of the hypothalamus and have wide projections throughout the brain (31). Histamine is one of the neuronal mediators, which are extensively released following TBI. It is known to play a role in the development of brain edema as it increases the vascular permeability and water content in the brain (32). The source of histamine after TBI remains speculative. Overactivation of the histaminergic system causes a gradual increase of histamine following the insult (31). In addition, external forces to the skull activate mast cells, causing them to release stored histamine and thereby exacerbating the brain injury (32). Three histamine receptors (H1R, H2R and H3R) are expressed in abundance in the brain. These receptors belong to the family of G-protein coupled receptors where ligand binding activates several second messengers pathways (33). Histamine binding on H1R activates the phospholipase C pathway, promoting inositol trisphosphate-dependent calcium release and diacylglycerol-sensitive activation of PKC (34). H2R activation stimulates adenylyl cyclase and augments intracellular cAMP, in turn activating PKA. H3R plays a role in the regulation of the synthesis and release of histamine (34).

The link between histamine and AQP4 was provided by Carmosino et al (2001, 2007). They showed that the number of OAP in AQP4-expressing gastric cells after histamine challenge was markedly reduced (35, 36). After histamine treatment, AQP4 is internalized where it relocates in late endosomes and recycles back to the plasma membrane after a histamine washout (35). This internalization is associated with an increased phosphorylation of AQP4 by PKA. However, this

phosphorylation takes place after AQP4 internalization where it cannot explain the direct effect on the plasma membrane water permeability (15). It has been suggested that PKA is involved in retaining AQP4 in a vesicle-recycling compartment inside the cells, which restricts the transmembrane water transport (15, 35). These findings suggest that histamine can consistently influence AQP4 function and localization in the brain. However, a conceivable correlation between both has not been established yet.

1.6 AQP4 membrane organization and dynamics

It has been postulated that AQP4 can be dynamically regulated by numerous stimuli, both in physiological and pathological conditions, allowing the cell to rapidly adjust their water permeability (15). Until recently, the only method to identify OAPs in cell membrane was the use of FFEM. Technical challenges of this technique and the necessity for fixation made it rather difficult to study OAP dynamics (37). Recently, blue native polyacrylamide gel electrophoresis has been demonstrated as an alternative to FFEM for OAP identification (38). However, the use of detergents precludes meaningful quantitative information about the OAPs (37). Advances in fluorescence microscopy have provided significant tools to study OAP dynamics quantitatively in the plasma membrane of living cells. In order to address questions about the regulation of OAP dynamics and membrane organization, the clustering in OAPs should be accurately determined. Therefore, diffusion can be exploited as a read-out parameter for OAP assembly as this higher-order organization impairs channel membrane diffusion (39). There are several microfluorimetric techniques available which are suitable for this purpose.

Fluorescence recovery after photobleaching (FRAP) is very straight-forward and well-established technique. Here, a high-intensity laser beam is used to bleach fluorescently labelled molecules in a region of the cell membrane. The recovery of the fluorescent signal in this region is measured, which represents the diffusion of non-bleached fluorescent molecules towards the bleached area. The recovery curve holds information on the diffusion process, with the subsequent analysis yielding a diffusion coefficient and mobile fraction **(figure 3A)** (40).

Techniques based on fluorescence correlation spectroscopy (FCS) can also be applied to study the aggregation of AQP4. Basically, FCS analyses the spontaneous temporal fluctuation of fluorescence intensity in a very small area or volume defined by a focused laser beam (41). These fluctuations arise from various processes which occur on the molecular level such as changes in local concentration due to motion in and out the sample volume or changes in their physicochemical properties, for example due to supramolecular aggregation (41, 42). These processes modulate the fluorescence intensity at a typical time scale, which can be derived from the autocorrelation function of the intensity trace. OAP assembly can induce important changes at the molecular level, which can be detected with FCS. FCS yields two useful parameters: (i) the detected fluorescence intensity or the brightness which can alter due to association/dissociation; and (ii) the diffusion coefficient **(figure 3B)** (40, 41). Spatial fluorescence fluctuations can be employed for either static or dynamic measurements in, respectively, image correlation spectroscopy (ICS) and temporal image correlation spectroscopy (TICS).

ICS can be used to study AQP4 densities or aggregation states. ICS analyses the spatial fluctuations around the mean fluorescence intensity within an image through the calculation of their spatial autocorrelation function. It does not yield information about the dynamics since the water channels are fixed during image acquisition (43). TICS is suited to study AQP4 dynamics as it permits the determination of the diffusion coefficient and flow speed of slow moving membrane proteins (42). The time course and the spatial dependency of the fluctuations is used to describe molecular properties including dynamics, number densities and the fraction of fluorophores which are immobile on the time scale of measurement (44).

Total internal reflection fluorescence (TIRF) microscopy can be used to study OAP formation at the bottom membrane of the cell in real time as it selectively excites fluorophores near the cell surface while minimizing fluorescence from intracellular regions. Therefore, a high signal to noise ratio is obtained. Moreover, exposure of light to the cell interior during image acquisition is minimized resulting in a markedly lower phototoxicity (45).

In FRAP, FCS based techniques and TIRF, the properties of a large number of particles are averaged. This can be problematic when the distribution of the molecular properties over the particles changes in time and/or space (46). Single particle tracking (SPT) involves the observation of the motion of individual particles (40). Linking the different positions of a particle over a series of time steps leads to the reconstruction of its trajectory. Information obtained from this trajectory can provide useful information of the molecular dynamics in the cell **(figure 3C)**. Calculation of the mean square displacement (MSD) indicates how far a particle has traveled within after a given time (46). The motional properties of the particle determine the profile of the MSD curve (40). SPT requires that the labeling density is sufficiently low. This allows a nanometer accurate determination of the molecule location by calculating the center of the observed point spread function.

1.7 Research hypothesis and experimental approach

In the present study, it was hypothesized that the astrocytic higher-order structure of AQP4 is disrupted after exposure to histamine. Initially, the feasibility for the use of microfluorimetric techniques in investigating the higher-order organization and dynamic behavior of AQP4 in the cell membrane was explored. A human 1321N1 astrocytoma cell line was used because of a negligible native AQP4 expression (47). Transient transfection of these cells was performed using c-Myc-tagged AQP4-M1 or Flag-tagged AQP4-M23 containing plasmids. In summary, immunofluorescence, FRAP, ICS and SPT were performed to characterize AQP4 membrane localization and dynamics. Furthermore, the effect of histamine exposure on the OAPs of AQP4 expressing cells was investigated using aforementioned techniques.

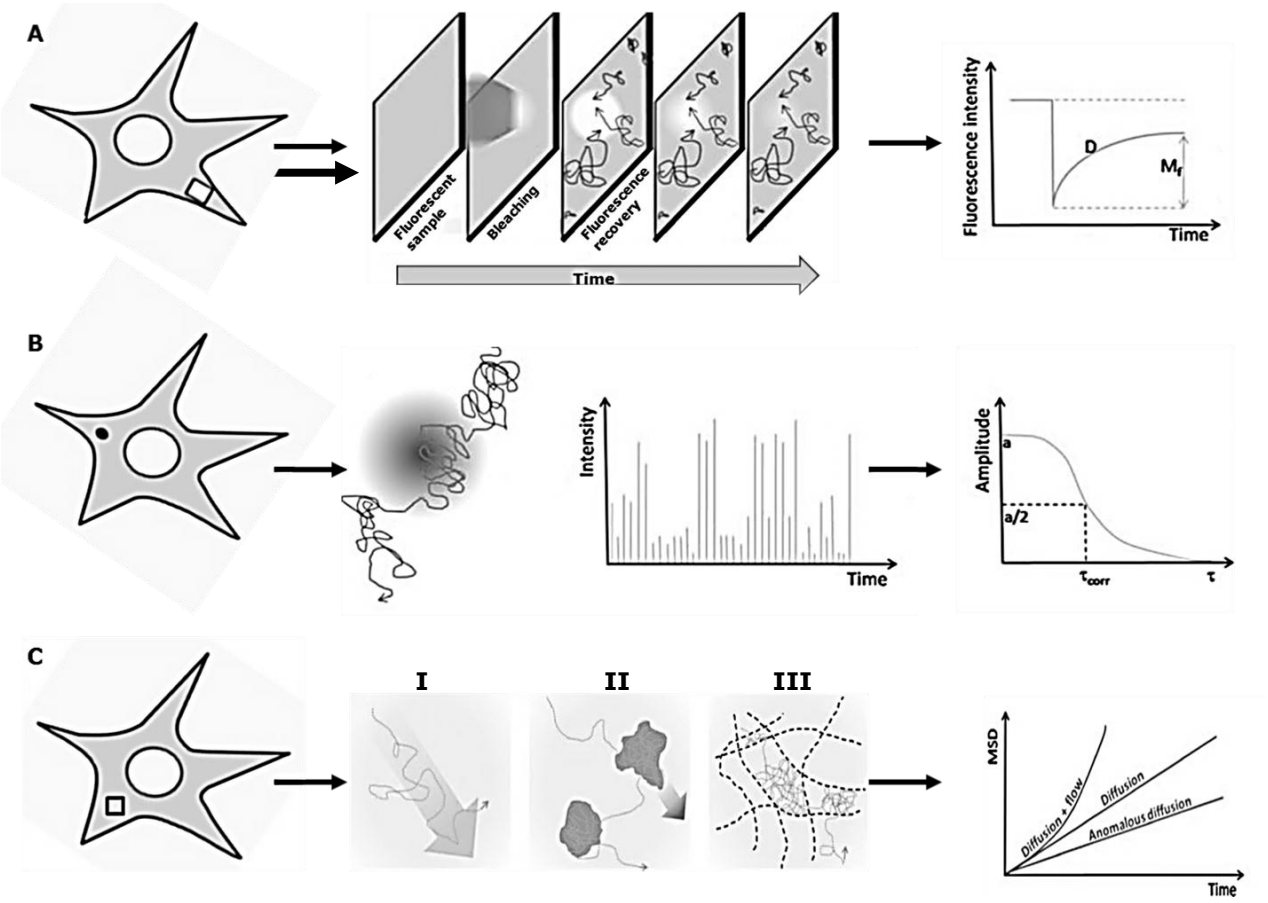

Figure 3: Microfluorimetric techniques for studying AQP4 dynamics. (A) Fluorescence recovery after photobleaching (FRAP) implies the selective bleaching of a region of the cell membrane (shown as a white square) with a high-intensity laser beam. By plotting the fluorescence signal over time, FRAP experiments are indicative for the diffusion coefficient D and the mobile fraction M_f. **(B)** Fluorescence correlation spectroscopy (FCS) and related techniques measure fluctuations in fluorescence intensity. Autocorrelation analysis of the fluctuations provides information about the mobility of the labeled molecules. **(C)** Single particle tracking (SPT) determines trajectories of single particles within the sample to obtain quantitative information regarding the motion mechanism of particles. Examples for fluorescent particle trajectories are shown: free diffusion (I), transient confinement in membrane microdomains (II) and confinement due to sub-membrane cytoskeleton meshwork (III). The time dependence of the mean square displacement (MSD) is indicative of the motional properties of the particle. *Adapted from Owen et al, 2009 (40).*

Chapter 2: Materials and methods

2.1 Astrocytoma cell culture

Human astrocytoma 1321N1 (HA) cells were kept in culture at 37°C under 5% CO_2 in Dulbecco's modified eagle's medium (DMEM; Gibco, Paisley, United Kingdom) supplemented with 10% fetal bovine serum (Biochrom AG, Berlin, Germany), 2% 200 mM L-glutamine (Gibco) and 2% sodium bicarbonate (Gibco). DMEM of stable transfected HA cell lines with AQP4-M1, AQP4-M23 or both were supplemented with, respectively, 100 µg/ml hygromycin (Invitrogen, Merelbeke, Belgium) or/and 400 µg/ml geneticin (Gibco). For routine passaging, cells were washed with Dulbecco's phosphate-buffered saline (Gibco) and detached using trypsin (Sigma-Aldrich, Ayrshire, United Kingdom) for 30 seconds. After incubating the cells at 37°C under 5% CO2 for 5 minutes, they were resuspended in DMEM and split retaining a 1:5 ratio.

2.2 Transfection of AQP4-M1 and AQP4-M23

2.2.1 Transient transfection

One day prior transfection, HA cells were seeded on 12 mm coverslips (Menzel-Gläser, Braunschweig, Germany) in twenty-four-well plates (Greiner Bio-One, Wemmel, Belgium) with a density of 50,000 cells per well and in eight-well Lab-Tek™ Chambered Coverglasses (Nunc, Roskilde, Denmark) with a density of 35,000 cells per well. DNA constructs encoding human AQP4-M1 and AQP4-M23 with a c-Myc (EQKLISEEDL) or Flag® (DYKDDDDK) epitope introduced at the second extracellular loop between residues 141 and 142 respectively, were ligated into mammalian expression vector pcDNA3.1 (Geneart AG, Invitrogen). Transfection was performed using Lipofectamine® 2000 Transfection Reagent (Invitrogen) according the manufacturer's protocol by means of 0.2 µg DNA/cm² and a 1:3 DNA Lipofectamine® 2000 Transfection Reagent ratio. Experiments were performed 24-48h post-transfection.

2.2.2 Stable transfection

Overexpressing cell lines were created by transfection using Lipofectamine® 2000 Transfection Reagent as described previously. DNA constructs encoding human AQP4-M1 and/or AQP4-23 were ligated into mammalian expression vector pcDNA3.1 which have, respectively, a hygromycin and geneticin resistance marker. Cells were seeded in petri dishes with a density of 10,000 cells/cm² in specific growth medium DMEM (Gibco). The cells were incubated overnight at 37°C under 5% CO_2. Subcloning was performed by limiting dilution. If a clone was isolated, it was further cultivated and tested for AQP4 expression and intracellular distribution.

2.3 Microscope instrumentation

Images were acquired using an epifluorescence Axiovert 200M equipped with a Zeiss LSM 510 Meta confocal laser scanning microscope (CLSM, Zeiss, Jena, Germany) and with a Plan-Neofluar 40x/1.3 oil immersion objective (Zeiss), a LD C-Apochromat 40x/1.1 W Korr UV-VIS-IR objective (Zeiss) and a αPlan-Apochromat 100x/1.43 oil immersion objective (Zeiss), placed on a vibration isolation table in an air-conditioned room kept at constant temperature. In live cell experiments, cells were kept at 37°C by the means of a small stage incubator (Tempcontrol 37-2 digital, PeCon, Erbach, Germany). The fluorophore Alexa Fluor® 488 was excited with the 488 nm line of an argon ion laser. The excitation light was directed to the sample using a main dichroic (DC) beam splitter (HFT 488). The emission light was directed through the DC and a secondary DC beam slipper (NFT) 490 and a band-pas (BP) 500-550 emission filter to the photomultiplier tube (PMT, Hamamatsu, Massy, France). The fluorophore Alexa Fluor® 555 was excited with the 543 line of a helium neon laser. The excitation light was directed to the sample using a HFT 543. The emission light was directed through the DC, a NFT 545 and a BP 565-615 to the PMT. The fluorophore Alexa Fluor® 647 was excited with the 633 nm line of a helium neon laser. The excitation light was directed to the sample using a HFT 633. The emission light was directed through the DC, a NFT 545 and a BP 650-710 to the PMT. The obtained images were analyzed using Zeiss LSM Image Browser (Zeiss), ImageJ software (National Institutes of Health, Bethesda, USA) and MATLAB (The MathWorks, Eindhoven, The Netherlands).

2.4 Immunofluorescence

Transfected HA cells were fixed in 4% (w/v) paraformaldehyde (PFA) in phosphate buffered saline (PBS) for 15 minutes. Afterwards, they were rinsed with PHEM buffer containing a final concentration of 5 mM PIPES, 2 mM EGTA, 2 mM $MgCl_2$ and Double Hanks consisting of 5.55 mM glucose, 5.36 mM KCl, 137 mM NaCl, 0.44 mM KH_2PO_4 and 4.15 mM $NaHCO_3$. Thereafter, HA cells were permeabilized using 0.5% Tween 20 (Sigma) in PHEM for 15 minutes. Next, they were incubated with blocking buffer containing 1% bovine serum albumin (BSA; Sigma), 6 mM glucose and 1 mM pyruvate in PBS for 1 hour at room temperature. Next, primary antibodies were incubated overnight by 4°C diluted in blocking buffer **(table 1)**. After 3 rinses with 1% BSA in PBS, the fluorescent labeled secondary antibodies diluted in blocking buffer were applied for 1 hour at room temperature. Finally, HA cells were rinsed extensively with 1% BSA in PBS and coverglasses were mounted with Vectashield® mounting medium containing 4',6-diamidino-2-phenylindole (Vector Laboratories, Peterborough, United Kingdom).

2.5 Visualization of late endosomes

HA cells were transducted with CellLight® Late Endosomes – Red Fluorescent Protein (Molecular Probes, Invitrogen) according to the manufacturer's protocol. The amount of particles per cell used to determine the volume of transduction reagent was 30. Experiments were performed 24-48h post-transduction.

Table 1: Overview antibodies

	Company	Product code	Concentration [µg/ml]
Primary antibodies			
Mouse anti c-myc	Sigma-Aldrich	M4439	2
Mouse anti Flag®	Sigma-Aldrich	F3165	7.6
Rabbit anti Flag®	Sigma-Aldrich	F2555	156
Rabbit anti AQP4 (h-80)	Santa Cruz Biotechnology	sc-20812	1
Secondary antibodies			
Alexa Fluor® 488-conjugated goat anti mouse	Invitrogen	A11029	10
Alexa Fluor® 555-conjugated goat anti rabbit	Invitrogen	A32162	10
Alexa Fluor® 647-conjugated goat anti rabbit	Invitrogen	A21245	10

2.6 Fluorescence recovery after photobleaching

Transfected HA cells were incubated with mouse anti c-myc and rabbit anti Flag® for 15 minutes diluted in DMEM without phenol red (MWPR; Gibco), which were fluorescent labeled using the Alexa Fluor® 488 Monoclonal Antibody Labeling Kit (A10235, Molecular Probes, Invitrogen) according to the manufacturer's protocol. The degree of labeling was determined using a Nanodrop ND-1000 spectrophotometer (Thermo Scientific, Wilmington, USA), resulting in 1 mole dye per mole mouse anti c-myc and in 4 mole dye per mole rabbit anti Flag®. After three washes with MWPR, FRAP measurements were proceeded. Spot photobleaching was performed for 614.4 ms with 100% laser output using a circular region of interest (ROI) with a radius of 2.5 µm. Pinhole size was set to 100 µm. Image size was typically set to 512x512 pixels with a pixel size of 60 nm. Each time series typically comprised 3 pre-bleach frames and 20 recovery frames.

Data extraction was performed in MATLAB using custom written routines. First, the coordinates of the circular bleach ROI were obtained from the metadata of the image sequence. Next, all pixels within the ROI were integrated frame by frame. The raw recovery curve $F_r(t)$ was extracted by calculating the average pixel intensity within the bleach ROI for each frame. Thereafter, the fluorescence intensity is corrected using a reference region to correct for instrumental fluctuations and photobleaching during image acquisition. Ensuing, the ROI fluorescence intensity was normalized to background intensity to correct for any intensity contribution due to instrumental or biological origin. Finally, the recovery values were normalized to the mean pre-bleach intensity. The resulting recovery curve $F(t)$ was fit to a standard exponential equation, where the fitted parameter M_f represents the mobile fraction and 1-M_f the immobile fraction IM_f [Eq. (1)].

$$F(t) = M_f(1 - e^{-\left(\frac{t}{\tau_D}\right)}) \quad (1)$$

If FRAP occurs by lateral diffusion, τ_D represents the characteristic diffusion time, which is proportional to the illuminated area [Eq. (2)]: where ω² represents the radius of the photobleached region and D the lateral diffusion coefficient (48).

$$D = \frac{\omega^2}{4\,\tau_D} \quad (2)$$

2.7 Image correlation spectroscopy

Transfected HA cells were labeled by two different methods, either labeling on living or fixed cells. In the first method, they were incubated for 1h at 37°C under 5% CO_2 with antibody solution diluted in DMEM. Afterwards, they were rinsed three times with DMEM and two times with PBS. Subsequently, they were fixed using 4% PFA in PBS. After three rinses with PBS, they were incubated with blocking buffer for 1 hour at room temperature. Next, the fluorescent labeled secondary antibodies diluted in blocking buffer were applied for 1 hour at room temperature. In the second method, they were labeled as described in section *2.4 Immunofluorescence*. In both methods, cover glasses were mounted with ProLong® Gold Antifade Reagent (Molecular Probes, Invitrogen).

The fluorophore Alexa Fluor® 488 was excited using a 150 fs pulsed laser light of a two photon Ti:Sapphire laser (MaiTai, Spectra-Physics, Utrecht, The Netherlands) tuned at an output wavelength of 930 nm. The emission light was detected using non-descanned detection: the fluorescence was directed using a short-pass (KP) 685 and a BP 495-545 towards a PMT. This PMT was connected to an SPC830 card (Becker & Hickl, Berlin, Germany) which also received the scan pulses from the CLSM. The resulting images have a 512 by 512 resolution, a pixel size between 10-30 nm and a pixel dwell time of 102 µs.

The recorded images were processed to determine AQP4 distribution parameters, namely, particle density (ρ) which represents the number of particles per µm², and degree of aggregation (A) – which is the average of fluorescent particles within a cluster. Spatial autocorrelation function was determined as described previously (43, 49): where the angular brackets denote spatial averaging over the image, and ξ and η are spatial lag variables corresponding to pixel shifts of the image relative to itself in *x* and *y* directions [Eq. (3)].

$$r\,(\xi,\eta,0)_t = \frac{\langle \delta i(x,y,t)\delta i(x+\xi, y+\eta, t)\rangle}{\langle i(x,y,t)\rangle_t^2} \tag{3}$$

The spatial autocorrelation function was calculated using Fourier methods [Eq. (4)], where $\mathcal{F}$ denotes the 2D spatial Fourier transform, $\mathcal{F}^*$ the complex conjugate of this transform and $\mathcal{F}^{-1}$ is the inverse 2D spatial Fourier transform.

$$r\,(\xi,\eta,0)_t = \frac{\mathcal{F}^{-1}|\mathcal{F}(i(x,y,t))\mathcal{F}^*(i(x,y,t))|}{\langle i(x,y,t)\rangle_t^2} - 1 \tag{4}$$

Next, the correlation function was fitted to a two-dimensional Gaussian function using a three parameter nonlinear least squares algorithm [Eq. (5)]:

$$r(\xi,\eta,0)_t = g(0,0,0)_t \exp\left(-\frac{\xi^2+\eta^2}{\omega^2{}_0}\right) + g_{\infty.t} \tag{5}$$

where $r(\xi,\eta,0)_t$ is the spatial correlation function of position ξ and η; $\omega_0$is the e^{-2} radius of the laser beam and $g(0,0,0)_t$ is the amplitude of the correlation function at the origin. The $g_{\infty.t}$ component is included to account for any non-zero correlation at large correlation distances due to the finite dimensions of the image.

The average number of independent fluorescent particles (N) in the observation area was calculated as the inverse of $g(0,0,0)$. Conversion of N towards the particle density ρ was performed by dividing by the effective area πω² of the observation area [Eq. (6)].

$$\rho = \frac{N}{\pi\omega_0^2} = \frac{1}{\pi\omega_0^2\, g(0,0,0)} \tag{6}$$

The degree of aggregation (A) was determined by dividing the average fluorescence intensity per particle by the average fluorescence intensity per monomer ε_m [Eq. (7)].

$$A = \frac{\langle i \rangle}{\varepsilon_m\ \rho} \tag{7}$$

2.8 Single particle tracking

Transfected HA cells were fluorescent labeled with Alexa Fluor® 488 diluted in MWPR for 15 minutes. Images were acquired using a Zeiss LSM 510 Meta CLSM: pinhole size was set to 200 µm. Image size was typically set to 512x512 pixels with a pixel size of 90 nm. Each time series typically comprised 120 frames with a frame time of 491,52 msec. Images sequences were analyzed and trajectories constructed using home-written routines in MATLAB. Briefly, for each trajectory the MSD, $\langle r^2(t)\rangle$, was calculated [Eq. (8)]:

$$\langle r^2(n\delta t)\rangle = \frac{1}{N-n}\sum_{j=0}^{N-n-1}([x(j\delta t + n\delta t) - x(j\delta t)]^2 + [y(j\delta t + n\delta t) - y(j\delta t)^2]) \tag{8}$$

where δt is the temporal resolution of the acquisition, $x(j\delta t)$and $y(j\delta t)$ represent the particle coordinate at time $t = j\delta t$, N is the total of frames recorded from an individual particle, and $n = 0, 1, 2, \ldots, N-1$. A linear least-squares fit to the first three points of the MSD versus t-curve, was performed to calculate the microscopic diffusion coefficient D_{1-3}[Eq. (9)].

$$\langle r^2(t)\rangle_{1-3} = 4D_{1-3}t \tag{9}$$

2.9 Histamine treatments

Cells were treated with 0.1 mM, 1 mM or 10 mM of histamine (Fluka, Steinheim, Germany) diluted in MWPR. As control, cells were exposed to MWPR. For the live cell imaging experiments, analyses were performed within a time frame of 45 minutes after histamine challenge. Other experiments were carried out on fixed cells, where cells were immediately fixed with 4% PFA after exposure. Afterwards, the classical immunocytochemistry protocol was followed.

2.10 Statistical analysis

Statistical analyses were conducted using GraphPad Prism 5 (GraphPad Software, La Jolla, USA). To determine whether the mean values were significantly different, the appropriate parametric unpaired Student's t-test with equal variances and non-parametric one-way analysis of variance (ANOVA) followed by Tukey test or Kruskal-Wallis test followed by Dunn's Multiple Comparison test was applied. P-values < 0.05 were considered statistically significant. All results were expressed as mean ± standard error of the mean (SEM).

Chapter 3: Results

3.1 Aggregation state of AQP4-M1 and AQP4-M23

In order to investigate whether AQP4 was able to form supramolecular aggregates in HA cells, transiently AQP4-M1 and AQP4-M23 transfected HA cells were characterized using immunofluorescence **(figure 4)**. AQP4-M1 transfected cells showed a diffuse staining pattern of the cell membrane, whereas AQP4-M23 showed a punctated pattern. This punctation indicates the ability to form supramolecular aggregates in HA cells **(figure 4A-B)**.

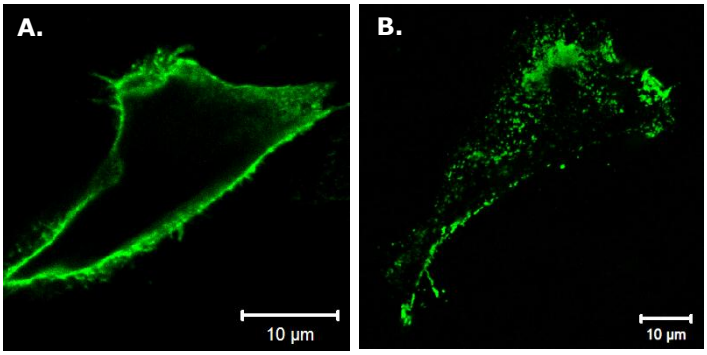

Figure 4: Characterization of cell membrane localization of AQP4 in transiently transfected HA cells. Immunofluorescence analysis of HA cells transfected with **(A)** AQP4-M1 and **(B)** AQP4-M23 showed, respectively, a diffuse and punctated staining pattern. *Scale bar: 10 µm.*

The aggregation states of AQP4 isoforms were further analyzed and quantified using ICS. Representative CLSM recordings of the bottom membrane are shown for AQP4-M1 and AQP4-M23 where a region of the bottom membrane of the cell was selected by increasing the zoom **(figure 5).** ICS analyses revealed that AQP4-M1 had a higher density compared to AQP4-M23 with on average five times more fluorophores per µm² **(table 2, figure 6)**. Furthermore, there was a fourfold difference in brightness with AQP4-M23 being the brightest. To determine the degree of aggregation, it was assumed that the fluorescent label Alexa Fluor® 488 had an equal brightness for each isoform and that this brightness was independent of the aggregation state. When each fluorescent entity of AQP4-M1 is assumed to represent to an individual AQP4-M1 tetramer, it can be concluded that each fluorescent entity of AQP4-M23 corresponds to an OAP containing on average twelve tetramers.

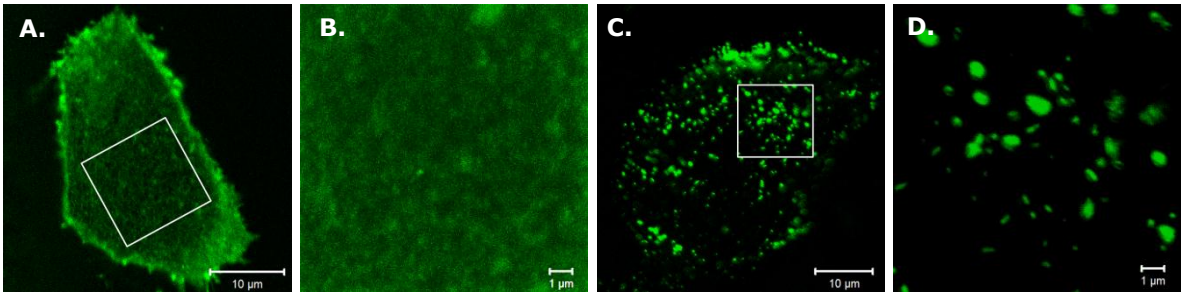

Figure 5: ICS measurement. Representative CLSM recordings of the bottom membrane of **(A-B)** AQP4-M1 and **(C-D)** AQP4-M23 transiently transfected HA cells. A region of the bottom membrane is selected by increasing the zoom, in order to avoid structures and cell edges which can interfere with the ICS analyses. *Scale bars: 10 µm for A, C; 1 µm for B, D.*

Table 2: Overview of ICS results

ICS analyses performed on transiently transfected HA cells expressing either AQP4-M1 or AQP4-M23. Particle density ρ and brightness ε were correct for background intensity and non-specific binding of antibody. Degree of aggregation A was presented as AQP4-M23 relative to AQP4-M1, where 1 equals one tetramer. N is the number of cells used for ICS analyses.

	ρ [particles/μm²]	ε [counts/particle]	A	N
AQP4-M1	8 ± 2	0.031 ±0.004	1	11
AQP4-M23	1.7 ± 0.2	0.12 ± 0.02	12 ± 2	19

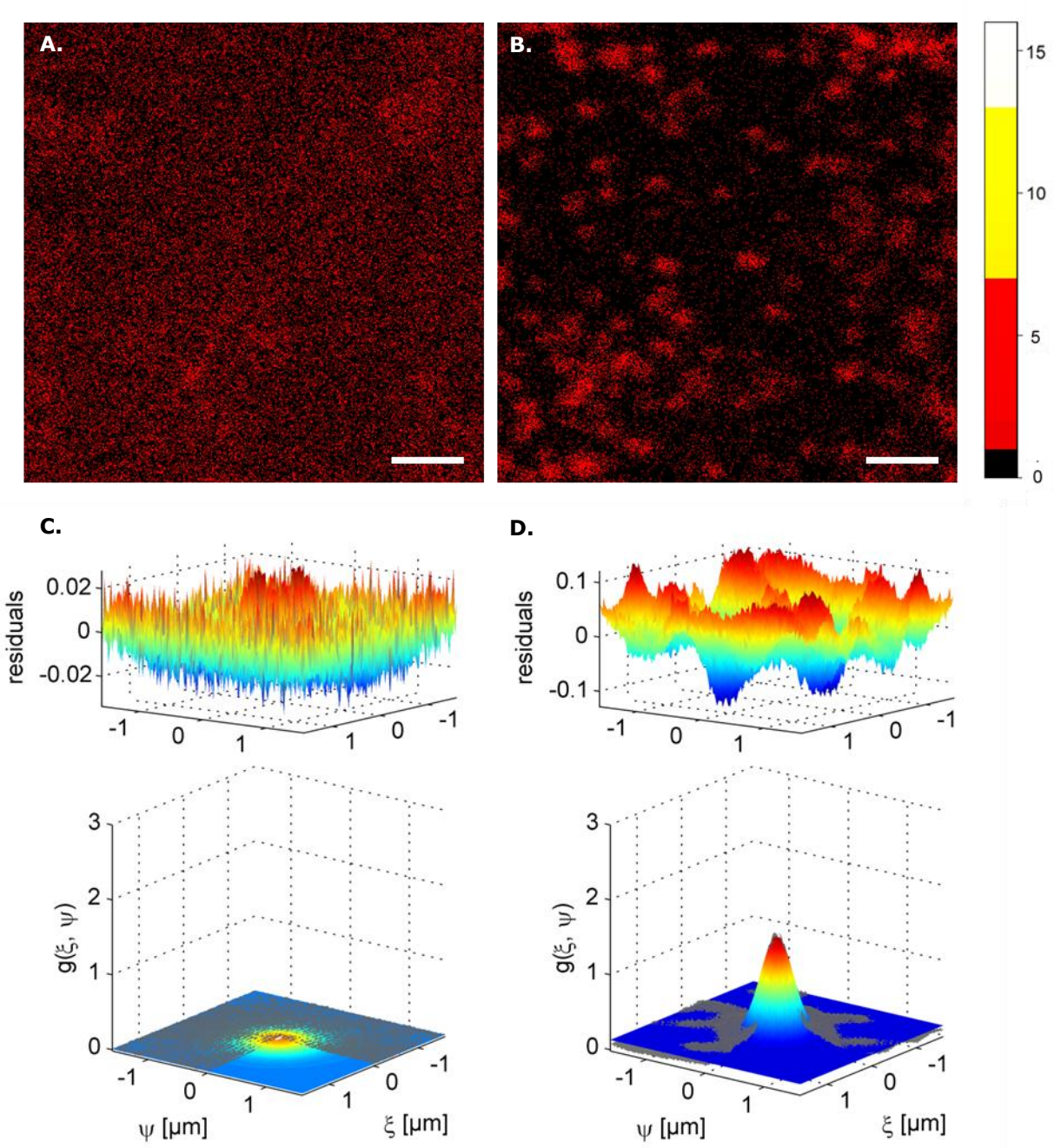

Figure 6: ICS analysis of AQP4-M1 and AQP4-M23. Representative images obtained **(A+C)** AQP4-M1 and **(B+D)** AQP4-M23 in fixed HA cells with their experimentally obtained spatial autocorrelation function together with the best fit (surface in rainbow colors). The residuals are above the corresponding SACF. Images have the same intensity scale as depicted by the color map (expressed in counts per pixels). *Scale bar: 2 μm.*

3.2 Mobility of AQP4

In order to determine the diffusion coefficient of AQP4-M1 and AQP4-M23, FRAP experiments were carried out **(figure 7)**. FRAP experiments using AQP4-M1 yield D = 0.038 ± 0.003 μm²/s. The corresponding mobile fraction of AQP4-M1 was 90 ± 4 %, which indicates that the majority of AQP4-M1 was mobile during the time frame of the measurement. FRAP experiments using AQP4-M23 were unsuccessful. Movement of bright clusters in and out the bleach ROI dramatically affected the recovery curve and renders it unsuitable for further analysis **(figure 6D)**. For that reason, SPT analysis was carried out for AQP4-M23.

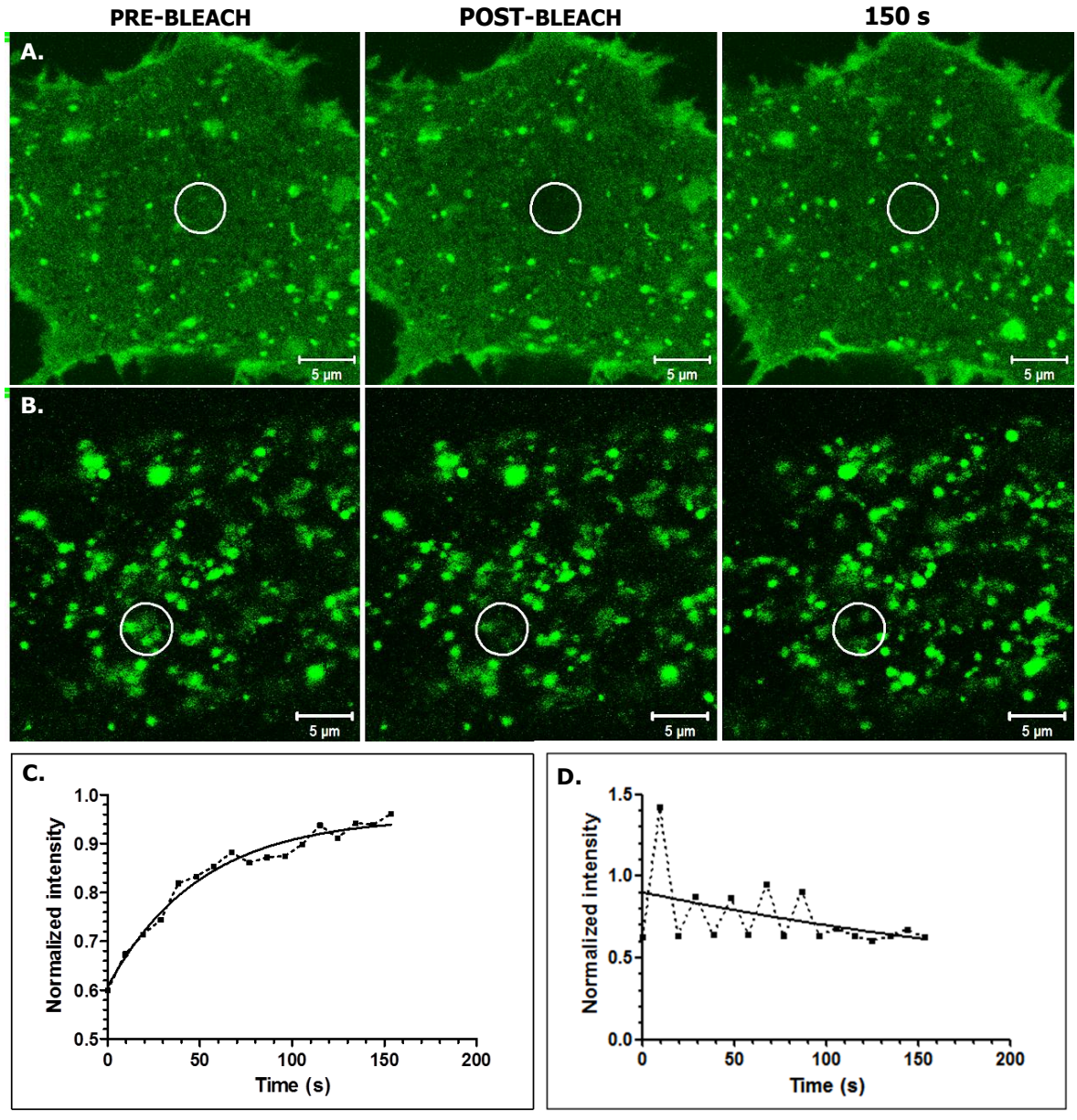

Figure 6: FRAP measurements in transiently AQP4 transfected HA cells. Representative CLSM recording from FRAP experiments for **(A)** AQP4-M1 and **(B)** AQP4-M23 transfected HA cells. Image sequence showing following events: before bleaching (pre-bleach), immediately after bleaching (post-bleach) and after 150 s. Bleach region is indicated with the circle. Images were collected at 10 s intervals. A typical observed recovery curve (dashed line) for **(C)** AQP4-M1 and **(D)** AQP4-M23 are shown together with a non-linear fit of the recovery curve (solid line). *Scale bar: 5 μm.*

A typical CLSM recording of AQP4-M23 transfected HA cells with their trajectories respectively is shown **(figure 8A-B)**. Single trajectories with a minimum of twelve time steps were analyzed. The microscopic diffusion coefficient was determined by fitting the first three points of MSD. The resulting diffusion coefficients from different recordings were pooled and averaged **(figure 8C)**. In summary, the average diffusion coefficient of AQP4-M23 is 0.0035 ± 0.0001 µm²/s.

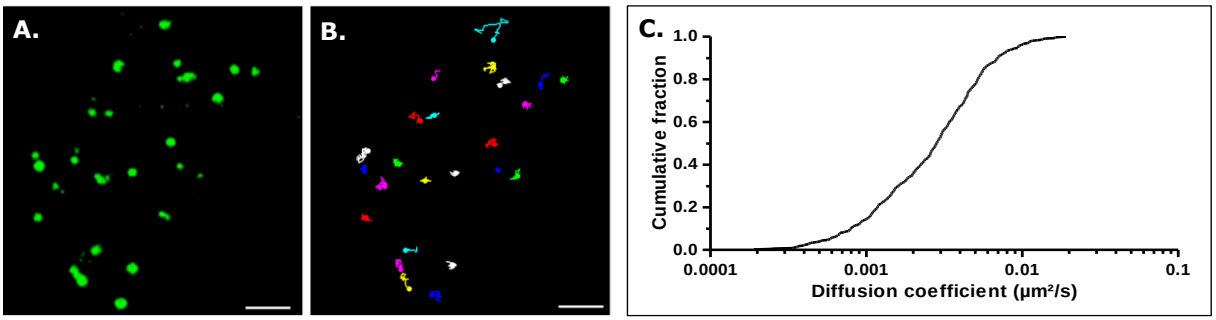

Figure 8: SPT of transiently AQP4-M23 transfected HA cells. (A) Representative CLSM recording of HA cells at 37°C labeled with Alexa Fluor® 488 conjugated rabbit anti Flag® antibodies. Time series of 120 frames were recorded at a frequency of 2 Hz. **(B)** Corresponding trajectories of the fluorescent labeled particles, visualized using ImageJ software. *Scale bar: 5 µm.* **(C)** Range of diffusion coefficients presented as a cumulative probability plot based on 497 trajectories. The average diffusion coefficient of AQP4-M23 is 0.0035 µm²/s.

3.3 Histamine induced AQP4 internalization

In order to investigate the effect of histamine on AQP4 localization in HA cells, AQP4-overexpressing cell lines were challenged with histamine and immunofluorescence was carried out **(figure 9)**. Cells were exposed to 0.1 mM, 1 mM or 10 mM histamine for either 5, 15 or 45 minutes. MWPR was used as a control. After 5 minutes, there was no difference between the several groups (data not shown). Nevertheless, after 15 and 45 minutes exposure an increased intracellular staining of AQP4-M23 and AQP4-M1+M23 overexpressing lines was found. A dose and time dependent response of histamine found. AQP4-M1 overexpressing lines only showed a moderate effect on histamine exposure.

To identify the mechanism by which histamine induces a translocation from the cell membrane towards the cytoplasm, stable overexpressing and transiently transfected HA cells were transduced with the late endosome marker Rab7a conjugated with red fluorescent protein **(figure 10-11)**. Co-localization was found in AQP4-M23 and AQP4-M1+M23 overexpressing cells. Nevertheless, the fluorescent signal of Rab7a was overwhelming in all conditions compared to AQP4, which makes it difficult to draw conclusions. No colocalization between Rab7a and AQP4 was found in the transiently transfected cells treated with histamine.

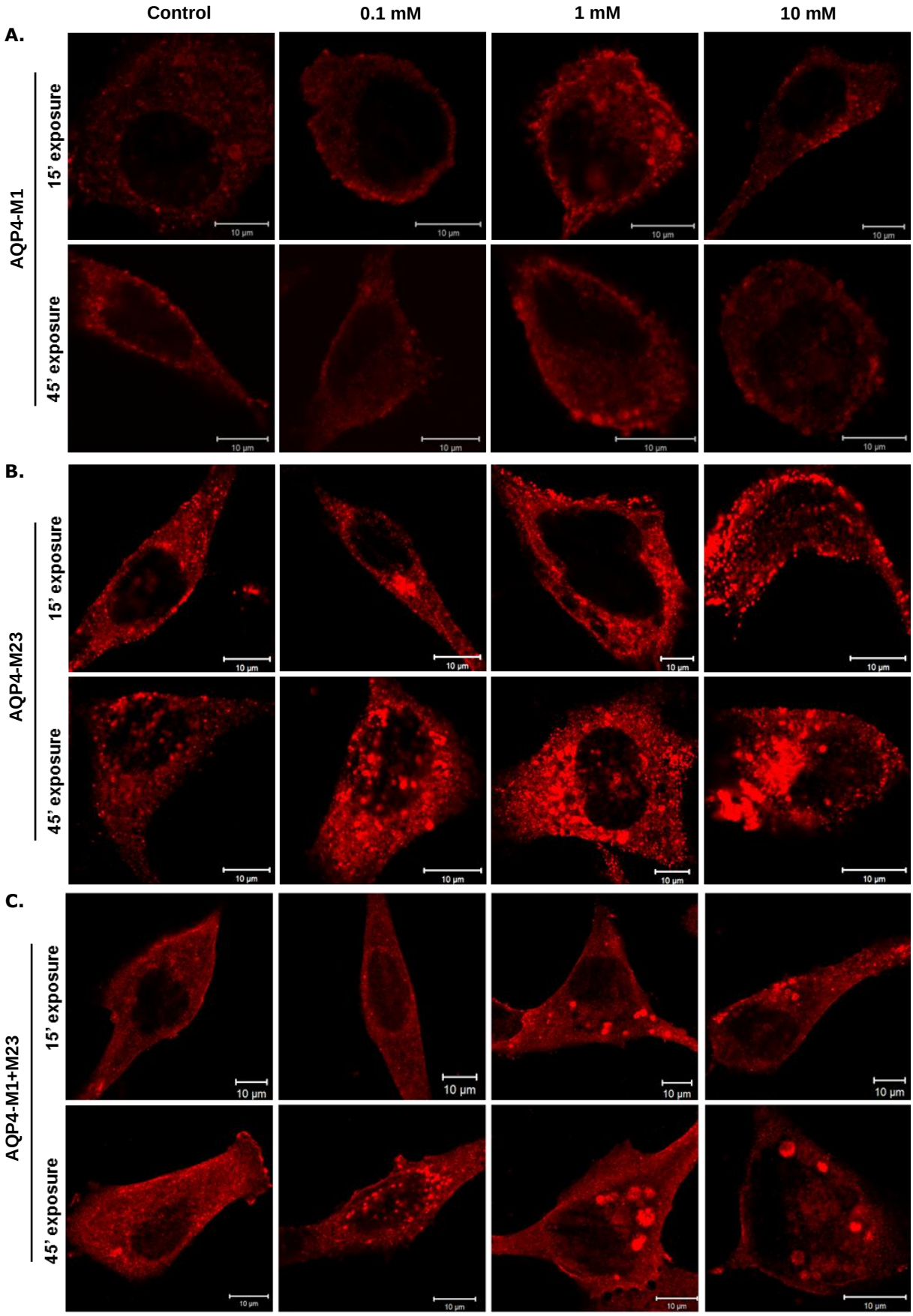

Figure 9: Histamine induced internalization of AQP4 overexpressing HA cells: (A) AQP4-M1, (B) AQP4-M23 and (C) AQP4-M1 + AQP4-M23. Representative recordings for each condition are shown. Each isoform was challenged to control solution (MWPR), 0.1 mM, 1 mM or 10 mM histamine for 15 or 45 minutes. Histamine mediated AQP4 translocation from the cell membrane towards the cytoplasm. Intracellular accumulation of AQP4 was found most prominently in AQP4-M23 overexpressing cells. *Scale bar: 10 µm.*

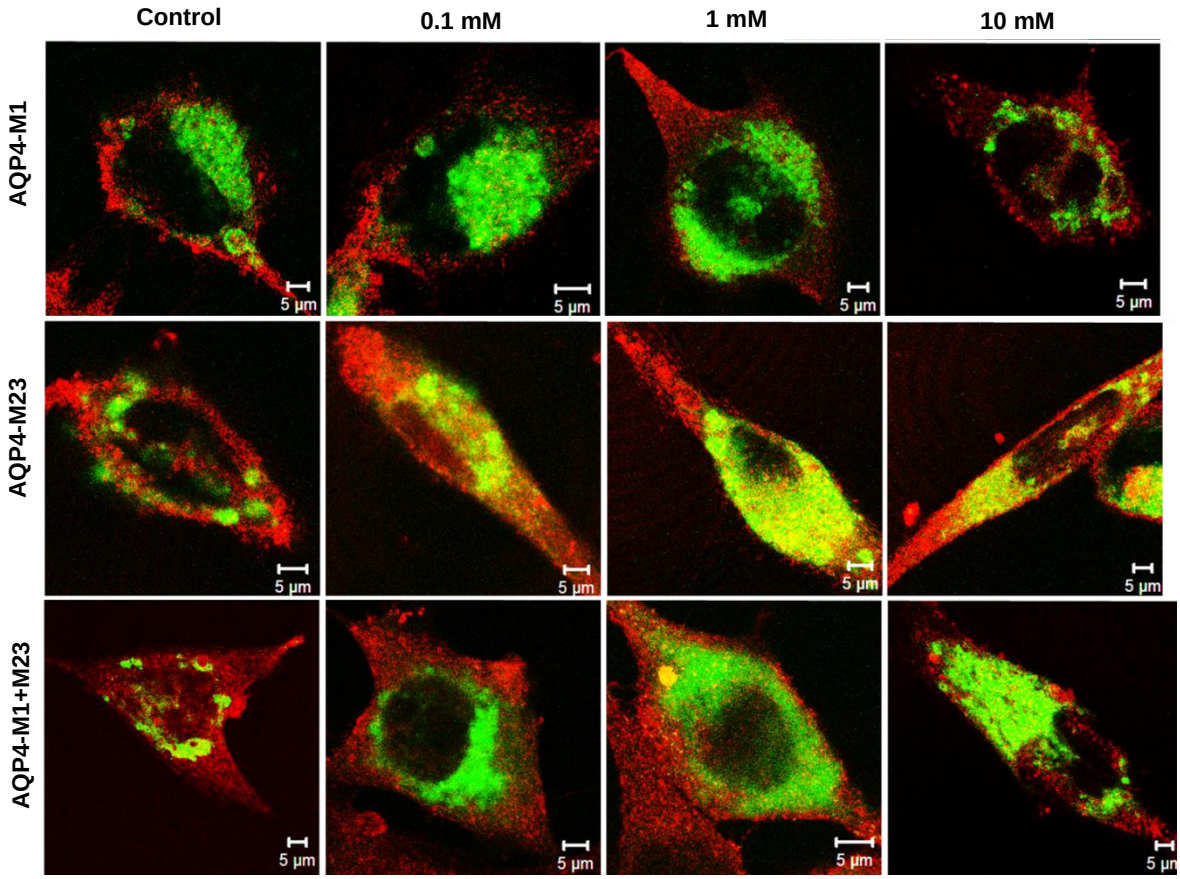

Figure 10: Histamine treatment on AQP4 overexpressing lines AQP4-M1, AQP4-M23 and AQP4-M1+M23, transduced with the late endosome marker Rab7a conjugated with red fluorescent protein (AQP4 shown in red, Rab7a in green). Representative recordings for each condition are shown. HA cells were challenged for 15 minutes of histamine with either 0.1 mM, 1 mM or 10 mM. MWPR served as a control. *Scale bar: 5µm.*

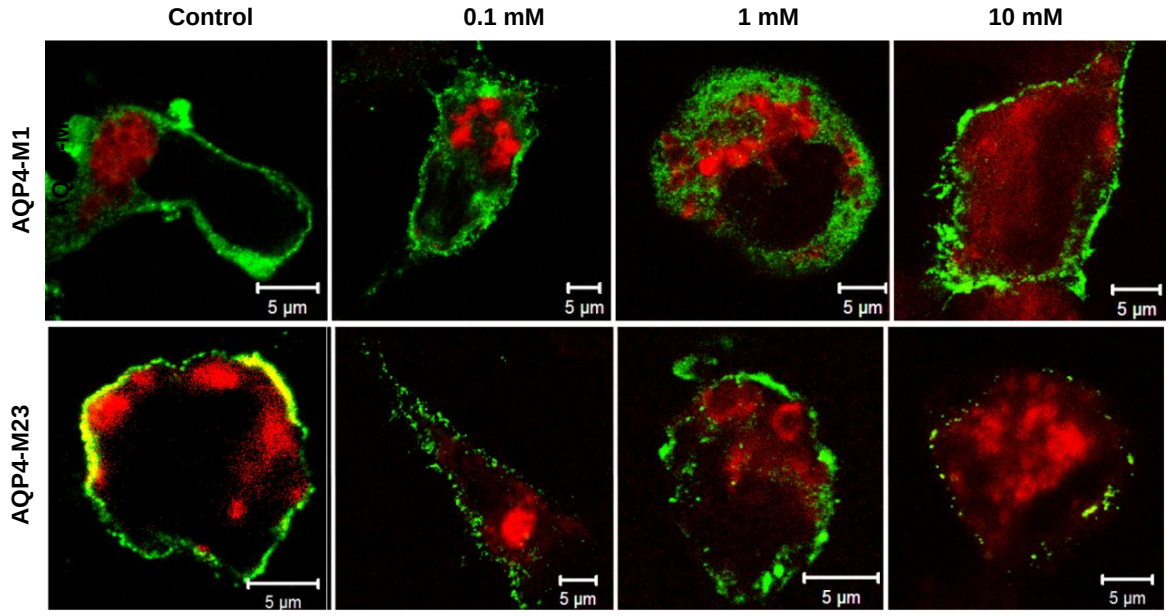

Figure 11: Histamine treatment on AQP4-M1 or AQP4-M23 transiently transfected HA cells transduced with the late endosome marker Rab7a conjugated with red fluorescent protein (AQP4 shown in green, Rab7a in red). Representative recordings for each condition are shown. HA cells were challenged for 15 minutes of histamine with either 0.1 mM, 1 mM or 10 mM. MWPR served as a control. No colocalization between AQP4 and late endosomes was found. *Scale bar: 5 µm.*

3.4 Histamine affects AQP4 supramolecular organization in OAPs

The effect of histamine on the aggregation state of AQP4 was analyzed and quantified using ICS **(figure 12, table 3)**. AQP4-M1 and AQP4-M23 transiently transfected cells were challenged for 15 minutes with 0.1 mM, 1 mM and 10 mM histamine. ICS did not found any difference between the density of AQP4-M1 and AQP4-M23 under the different conditions. On average, there were three times more fluorophores per µm² in AQP4-M1 compared to AQP4-M23. The brightness of the AQP4 isoforms did significantly change during the histamine challenge **(figure 13A).** AQP4-M1 had a significantly higher brightness after 10 mM histamine exposure *(Kruskal-Wallis, p=0.0008)*, but not at lower concentrations. In contrast, AQP4-M23 brightness reduced after 1 mM and 10 mM histamine exposure *(Kruskal-Wallis, p=0.0218)*. Compared to the physiological conditions **(table 2)**, the degree of aggregation of AQP4-M23 was significantly reduced after histamine challenge *(Kruskal-Wallis, p=0.0002)* (**figure 13B)**.

Table 3: Overview of ICS results
ICS analyses performed on transiently transfected HA cells expressing either AQP4-M1 or AQP4-M23 which were challenged with different concentrations of histamine for 15 minutes. Particle density ρ and brightness ε were correct for background intensity and non-specific binding of antibody. Degree of aggregation A was presented as AQP4-M23 relative to AQP4-M1, where 1 equals one tetramer. N is the number of cells used for ICS analyses.

	P [particles/µm²]	ε [counts/particle]	A	N
AQP4-M1				
0.1 mM	17 ± 2	0.024 ± 0.007	1	7
1 mM	25 ± 5	0.012 ± 0.005	1	7
10 mM	20 ± 3	0.186 ± 0.075	1	10
AQP4-M23				
0.1 mM	5 ± 1	2.048 ± 0.4	4 ± 2	10
1 mM	7 ± 2	0.9 ± 0.1	1.9 ± 0.7	10
10 mM	6 ± 2	0.8 ± 0.3	3 ± 2	9

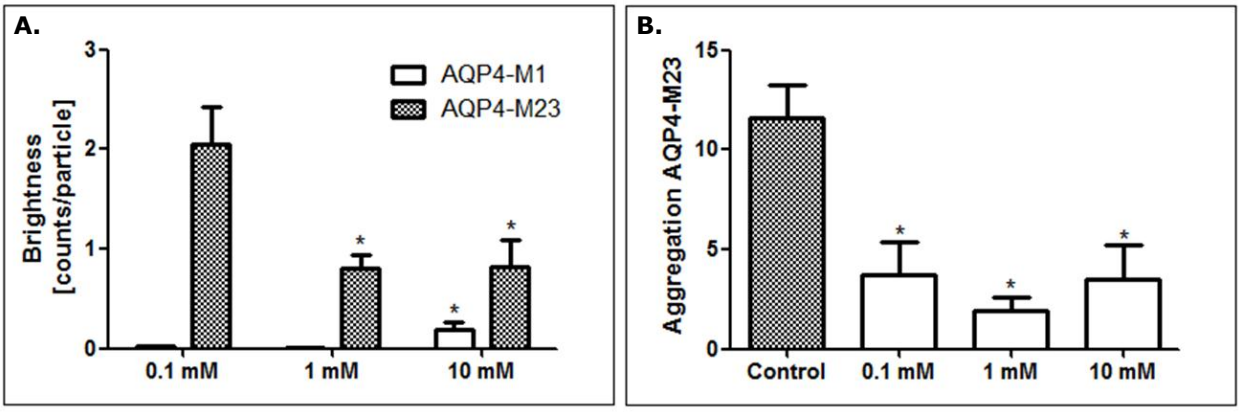

Figure 13: ICS analysis of AQP4-M1 and AQP4-M23. (A) The brightness ε of both AQP4 isoforms is shown. AQP4-M1 had a significantly higher brightness after 10 mM histamine exposure compared to the lower concentrations *(Kruskal-Wallis, p=0.0008)*. In contrast, AQP4-M23 brightness reduced after 10 mM histamine exposure *(Kruskal-Wallis, p=0.0218)*. **(B)** The degree of aggregation of AQP4-M23 was significantly reduced after histamine challenge compared to the control (*Kruskal-Wallis, p=0.0002)*.

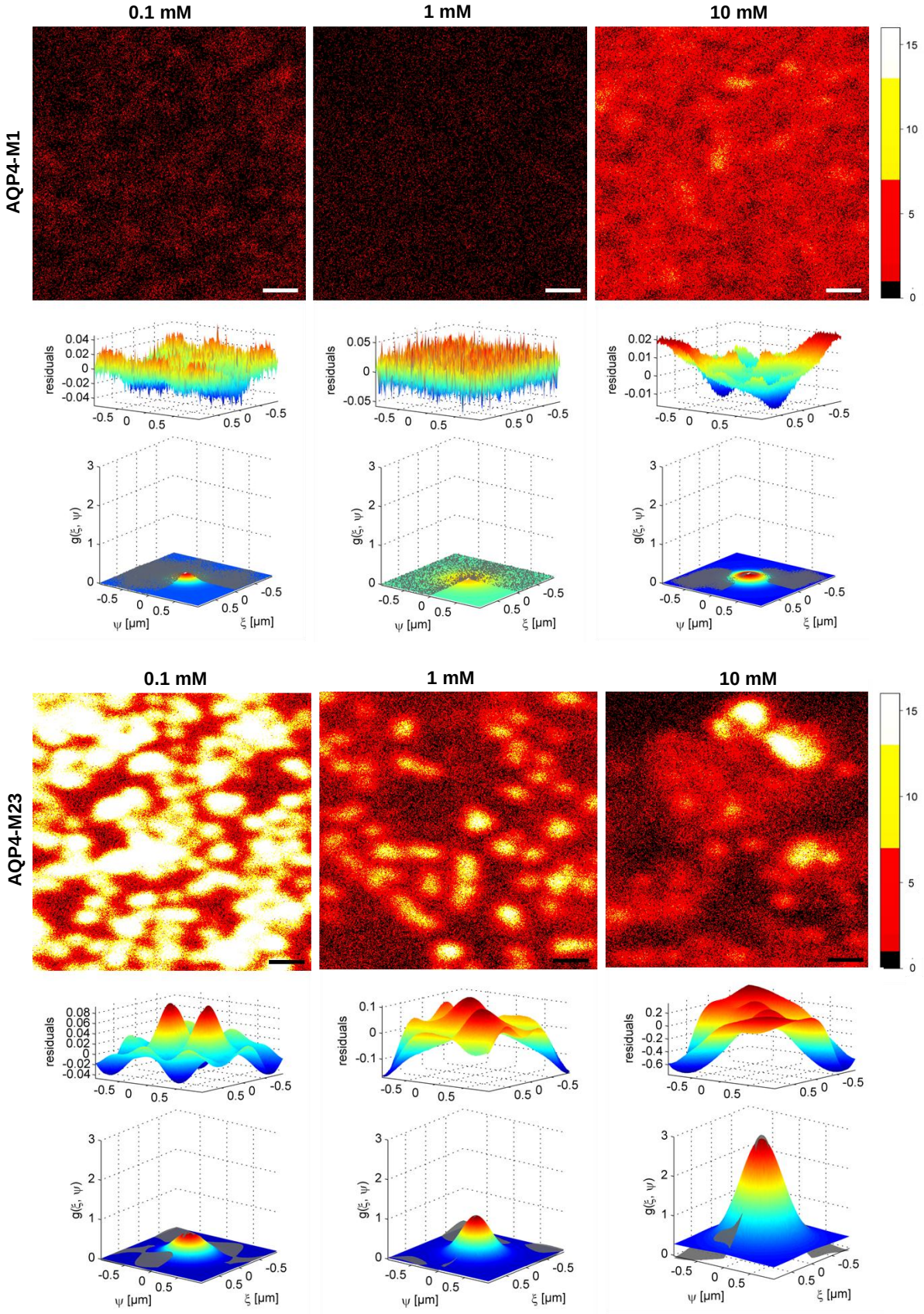

Figure 12: ICS analysis of AQP4-M1 and AQP4-M23 after histamine treatment. Representative images obtained AQP4-M1 (upper panel) and AQP4-M23 (lower panel) in fixed HA cells after 15 minutes histamine challenge. The experimentally obtained spatial autocorrelation function together with the best fit (surface in rainbow colors) is shown below each recording. The residuals are above the corresponding SACF. Images have the same intensity scale as depicted by the color map (expressed in counts per pixels). *Scale bar: 1 µm.*

Furthermore, the effect of histamine was studied using FRAP for AQP4-M1 and SPT for AQP4-M23. FRAP analysis revealed that 1 mM histamine treatment increased AQP4-M1 membrane diffusion, 0.0467 ± 0.004 µm²/s compared to control, 0.0384 ± 0.003 µm²/s *(unpaired Student's t test, p=0.0449)* **(figure 13A)**. However, the immobile fraction was not altered 0.14 + 0.03 in the control group to 0.13 + 0.02 in the histamine treated group **(figure 13B)**. SPT of AQP4-M23 was carried out where HA cells were treated with 1 mM histamine. The resulting SPT analyses were divided into two phases: early effect (1-15 minutes post-exposure) and delayed effect (15-30 minutes post-exposure). Histamine resulted in an increased diffusion coefficient with 0.0083 ± 0.0002 µm²/s for early effect and 0,0068 + 0,0002 µm²/s for delayed effect, compared to 0.0035 ± 0.0001 µm²/s in the control group (*ANOVA, p < 0.0001)*.

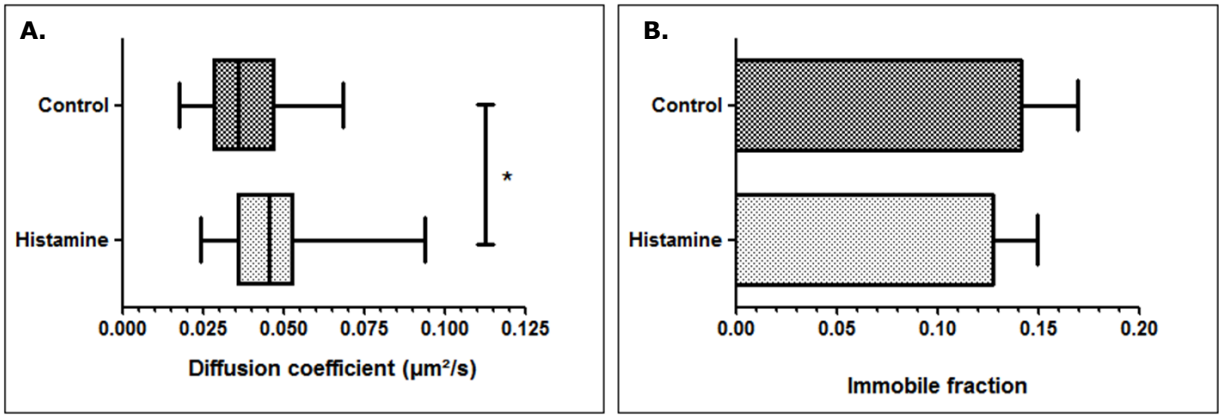

Figure 13: FRAP of transiently AQP4-M1 transfected cells treated with a control solution or 1 mM histamine. (A) Cumulative distributions of diffusion coefficients are shown. Diffusion coefficient of AQP4-M1 was significantly increased in histamine treated group, 0.047 ± 0.004 µm²/s (n=20), compared to control, 0.039 ± 0.003 µm²/s (n=24) *(unpaired Student's t test, p=0.045)*. **(B)** The immobile fraction was not altered: 0.14 + 0.03 (n=24) in the control compared to 0.13 + 0.02 in the histamine treated group (n=20).

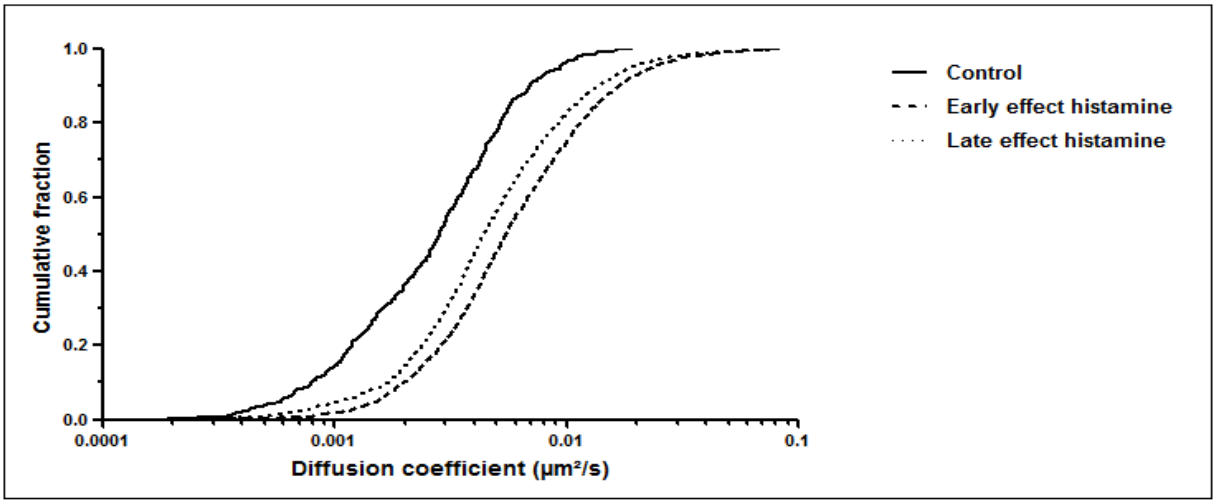

Figure 14: SPT of transiently AQP4-M23 transfected cells treated with a control solution or 1 mM histamine. Time series of 120 frames were recorded at a frequency of 2 Hz. The total amount of trajectories analyzed were 497 for the control, 1471 for the early effect and 1455 for the delayed effect. Cumulative distributions of diffusion coefficients are shown. The SPT data of the treated conditions were divided into two groups: early effect (between 1 and 15 minutes post-exposure) or delayed effect (between 15 and 30 minutes post-exposure). A clear shift of the cumulative distribution in the treated groups was found. Histamine increased diffusion coefficient towards 0.0083 µm²/s for early effect and 0.0068 µm²/s for delayed effect, compared to 0.0035 µm²/s in the control.

Chapter 4: Discussion

4.1 Microfluorimetric measurements as a tool for studying AQP4 supramolecular organization

In order to address questions about the regulation of OAP dynamics and membrane organization, clustering of AQP4 in OAPs should be accurately determined. AQP4 supramolecular organization was studied using several microfluorimetric techniques. Transient transfection of HA cells was performed using c-Myc-tagged AQP4-M1 or Flag®-tagged AQP4-M23 containing plasmids where the tags were introduced between residues 141 and 142 in the second extracellular loop of AQP4. Previous investigations have shown that insertion of the tags at this site did not affect AQP4 expression, membrane targeting or water permeability (14, 17).

4.1.1 Aggregation of AQP4

In order to obtain more information about the aggregation of AQP4 in OAPs, ICS analyses were carried out. AQP4-M1 did not form clusters in the cell membrane, whereas AQP4-M23 did form clusters with a density of 11 tetramers per cluster. FFEM studies showed that AQP4-M1 seemed to be randomly scattered throughout the cell membrane and AQP4-M23 formed OAPs ranging from 30 to 500 AQP4 tetramers per clustering (11, 50, 51). Nevertheless, it has to be underscored that antibody labelling of AQP4 molecules in our study probably underestimate the real composition of an OAP because steric hindrance may prevent access to all available binding sites (39). Previously, when fluorescence images were compared to FFEM, only one fluorescent labelled antibody was found for approximately 6 AQP4 epitopes. Accordingly, less than one binding event per AQP4 tetramer occurred (17). This could explain the observed discrepancy between our findings and previous FFEM investigations.

4.1.2 Mobility of AQP4

In the present study, by using FRAP analysis, AQP4-M1 had a diffusion coefficient of 0.038 $\mu m^2/s$ and a mobile fraction of 90%. In the literature, however, a diffusion coefficient of 0.050 $\mu m^2/s$ and a mobile fraction of ~ 80% was found (10, 37, 52). Because during all experiments FRAP was performed at 37°C, temperature cannot be responsible for the found discrepancy. Other factors can contribute to an inconsistency in diffusion coefficient. Previously, LLC-PK1 renal epithelial cells and HeLa cells were used for photobleaching experiments, where different membrane composition might result in a different membrane viscosity, thereby influencing AQP4-M1 diffusion. Another contributor to the discrepancy might be the AQP4 expression level. High protein levels may induce a declined diffusion coefficient due to macromolecular crowding. Previous investigations were principally performed on stably transfected cell lines, which express in general lower levels of protein compared to transient transfections. Hence, these differences in experimental set-up might explain why the observed diffusion coefficient is lower compared to those found in the literature.

In the present study, FRAP analysis of AQP4-M23 could not be performed precisely. Movement of bright clusters in and out the bleach ROI precludes an accurate reconstruction of the recovery curve. In order to circumvent this problem, large ROI sizes have to be considered. However, increased ROI sizes complicate FRAP measurements as they are accompanied with more border effects on the recovery signal and augmented total loss of fluorescence. Visual inspection showed that there was little movement of the AQP4-M23. Formerly, photobleaching was carried out for AQP4-M23 conjugated with GFP. Here, relatively little recovery of the fluorescent signal (less than 40%) was found (9). This implies that slow moving OAPs will probable reside in the immobile fraction. FRAP can therefore be expected to be relatively insensitive to detect the lower diffusion coefficient. Therefore, other techniques may be more suited to explore the dynamics of AQP4-M23. For that reason SPT was used to acquire quantitative information of AQP-M23 diffusion. Trajectory analyses revealed that AQP4-M23 motion was highly restricted, which is in accordance with the literature. Previously, it was shown that AQP4-M23 trajectories had a characteristic negative curvature, which is expected for confined or anomalous diffusion (39). The average diffusion coefficient in the present study was calculated to be 0.0035 $\mu m^2/s$, which is in contrast with the 0.0060 $\mu m^2/s$ found in literature (17). As mentioned previously, the dissimilarity in cell lines and expression system could be responsible for the observed discrepancy.

AQP4-M1 had one order of magnitude higher diffusion coefficient compared to AQP4-M23, which is similar to previous investigations (14, 17, 39). This difference can be, at least partially, explained by Einstein-Stokes equation, which states that the hydrodynamic radius of a particle is inversely related to the diffusion coefficient. ICS data showed that there was indeed a markedly difference in aggregation between both isoforms. Assembly in OAPs is to be expected responsible for the restricted diffusion of AQP4-M23.

AQP4-M1 and AQP4-M23 co-expression diffusion measurements were not included in this study. However, OAP sizes are reduced when AQP1-M1 is co-expressed with AQP4-M23, suggesting an interaction between these two isoforms (11). Using two-color SPT, a strong interaction of AQP4-M1 and AQP4-M23 was found. The ratio of AQP4-M1 to AQP4-M23 has a strong effect on AQP4 diffusion. This might reflect a shift in distribution of OAP sizes and the fraction of AQP4 molecules that diffuses as free tetramers (14). Nevertheless, it was shown the presence of AQP4-M1 to the OAPs rather than incorporation into OAPs was responsible for modulating AQP4-M23 motions (17).

4.2 Histamine affects AQP4 localization and supramolecular organization

In the present study, it was hypothesized that the astrocytic higher-order structure of AQP4 is disrupted after exposure to histamine. We were able to find a negative correlation between histamine and AQP4 in astrocytes using microfluorimetric approaches. Previously, Mertens et al and Nuydens et al (unpublished results) found that histamine treatment impaired hypotonicity induced cell swelling and affected the course of TBI in a rat animal model (53, 54).

4.2.1 Histamine challenge induced AQP4 internalization and disrupts AQP4 higher order organization in OAPs

The neuronal mediator histamine was shown to induce AQP4 internalization in a dose-dependent way. Histamine challenge induced a rapid translocation to the cytoplasm, which was more pronounced in AQP4-M23 cells compared to AQP4-M1. AQP4-M1 and AQP4-M23 co-expression resulted in an intermediate response to histamine. To further examine the origin of the intracellular vesicles, AQP4 overexpressing cell lines and transiently transfected cells were transduced using fluorescent late endosomes. AQP4-M23 and AQP4-M1+M23 overexpressing cells showed colocalization between AQP4 and Rab7a. Nevertheless, the fluorescent signal of Rab7a was overwhelming in all conditions compared to AQP4, which makes the precision of the measurement doubtful. No localization of AQP4 within the late endosomal compartment was found in the transiently transfected cells. These findings are in contrast with the observed endocytosis of AQP4-M1 in histamine treated gastric cells, where AQP4-M1 was localized with the late endosomal marker mannose-6-phosphate (35, 36). Our findings suggest that either AQP4 may endosomes already entered the degradation pathway or were accumulated in recycling endosomes. Nevertheless, no co-localization was previously found with the lysosomal-associated membrane glycoprotein AC17 in gastric cells (35). Further studies using the recycling endosome marker Rab11 could verify whether the endosomal pathways are involved in AQP4 internalization (55). This might be interesting because previously the majority of AQP4 was able to relocalize back to the cell membrane after histamine wash out (35). This would imply the effect of histamine is completely reversible.

ICS analysis revealed that AQP4-M1 brightness significantly increased after 15 minutes of 10 mM histamine exposure. This finding was unexpected. It may suggest that at this concentration clathrin-mediated endocytosis could be induced where the formation of coated pits loaded with AQP4-M1 may be responsible for this observation. AQP4-M23 showed a decreased brightness after 1 and 10 mM histamine exposure, which might indicate that the size of an OAP is reduced. Moreover, compared to the control situation histamine treatment induced a significant reduction of the aggregation state. AQP4-M1 diffusion enhanced after histamine challenge. As histamine could induce AQP4 internalization, less AQP4 molecules are present in the cell membrane and therefore macromolecular crowding may be minimized. Consequently, the mobility of AQP4-M1 tetramers in the plasma membrane was augmented.

SPT analysis of AQP4-M23 showed that after histamine challenge, diffusion was enhanced compared to control conditions, which was confirmed by the ICS measurements which showed that the degree of the aggregation in OAP was significantly reduced. Remarkably, in the early phase after histamine exposure the increased diffusion was significantly higher compared to that during the delayed phase. Histamine is known to mediate a desensitization response, explained by a rapid internalization of H1R after histamine challenge (56). Loss of functional H1R on the cell membrane may be responsible for the effects on diffusion and aggregation found in the delayed phase.

The different cell types used in the study of Carmosino et al and the present study might explain the dissimilarities in the reported results. Gastric HGT-1 cells only express the H2R, leading to the activation of PKA after histamine exposure (57). Histamine-induced AQP4 internalization was associated with an increase in AQP4 phosphorylation. Histamine stimulation resulted in a tenfold increase in phosphorylated AQP4 which was abolished by addition of a specific PKA inhibitor H89. However, addition of this PKA inhibitor was not able to block AQP4 internalization. In turn, specific PKC and CK2 inhibitors were not able to reduce AQP4 internalization or phosphorylation. These findings suggested that PKA is the kinase that is responsible for AQP4 phosphorylation. Furthermore, it was shown by Carmosino et al that AQP4 phosphorylation occurred subsequent to its internalization in late endosomes. PKA was proposed to be involved in retaining AQP4 in a vesicle-recycling compartment (35, 36). In contrast, HA cells, which were used in this study, were found to express the H1R, but not H2R or H3R (54). Histamine binding to H1R leads to the activation of PKC. In order to further elucidate the mechanisms involved, the addition of downstream inhibitors of H1R can be applied (e.g. PKC blockers). The relationship between of AQP4 regulation and PKC was already established in other cell types. Oocyte swelling assay and protein phosphorylation studies in rat brain homogenate revealed that PKC phosphorylation of AQP4 was able to reduce mediated water permeability (58). Moreover, in glioma cells phosphorylation of serine 180 leads to reduced water permeability where dephosphorylation enhanced water permeability (59). PKC dependent reduction of AQP4 water permeability was shown to be due to AQP4 internalization (16). AQP4-M23-expressing Xenopus laevis oocytes were significantly more sensitive to PKC activation than oocytes expressing the larger isoform AQP4-M1, which was accompanied with a more prominent AQP4 internalization. The selectivity for the AQP4-M23 isoform suggested a function for organization of AQP4 isoforms into large OAPs, where after phosphorylation the internalization machinery is able to retrieve more molecules AQP4 for each adaptor protein when AQP4 is organized into its supramolecular structure. This would allow a more efficient and dynamic regulation of the AQP4 mediated water permeability (16). These findings are in accordance with *in vivo* studies were activation of PKC, by administration of phorbol dibutyrate, in a rat model of TBI prevented traumatic brain edema. This finding was accompanied with a downregulation of AQP4 (60). Furthermore, treatment of phorbol 12-myristate 13-acetate in a model of focal ischemia induced by middle cerebral artery occlusion resulted in a downregulation of AQP4 in the ischemic area and a reduction in brain edema formation (61). These findings indicate that PKC is able to modulate AQP4 functionality.

4.2.2 Histamine impaired hypotonicity induced cell swelling

The findings in present study are in agreement with functional cell swelling assays previously performed by Mertens et al and Nuydens et al (53, 54). In this assay, naieve or transfected HA cells were loaded with the fluorescence dye calcein and a fluorescence based approach was used to measure changes in cell volumes after osmotic challenges. Pretreatment with histamine decreased dose-dependently the hypotonic induced cell swelling. Pretreatment with 10 mM histamine for 3 minutes was sufficient to impair hypotonicity induced cell swelling to a higher extent.

However, no difference between the AQP4-M1, AQP4-M23 or both isoforms was detected. In present study, translocation of AQP4 from the cell membrane illustrated after histamine challenge. Therefore, it can be concluded that AQP4 internalization results in an impaired transmembrane water flow.

4.2.3 Implications of histamine on the course of TBI and brain edema

Histamine is probably able to affect the course of TBI *in vivo*, as in a rat model intracerebroventricular injected histamine can modulate ICP changes on fluid infusion (Smets et al, unpublished results). Histamine addition during a standardized intracerebroventricular injection resulted in higher ICP values, which upon cessation of infusion did not return to baseline compared to the control injections without histamine. It was been suggested that histamine-induced AQP4 internalization compromised the removal of excess fluid and as such the changes in ICP.

Previously, other *in* vivo studies indicated that the expression pattern of AQP4 alters during TBI. Ke et al showed that a AQP4 negative immunostaining and downregulation of its mRNA was found in the edematous contusional cortex 24 hour post-injury, while AQP4 mRNA was upregulated in more distant regions (62). This is consistent with the results of Zhao et al, who showed that TBI decreased AQP4 level in the injury core and modestly increased in the region surrounding this core (63). In contrast, Sun et al presented an upregulation of AQP4 mRNA at the site of injury and downregulation adjacent to the site of injury. They suggested that upregulation of AQP4 may be accountable for the formation of brain edema following the injury. Downregulation adjacent to the injury site may protect the propagation of brain edema (64). Furthermore, in a rat model of penetrating brain injury AQP4 immunoreactivity was substantially increased in the injured tissue and adjacent regions which was suggested to be due to de novo AQP4 protein synthesis (65). Additionally, an increased expression of AQP4 in astrocytes of human contused brain at the injury site and upregulation of AQP4 after TBI in human was revealed (66, 67). These findings demonstrate dynamic spatial and temporal changes in AQP4 expression. Further investigations are necessary to elucidate these contractions. In general, AQP4 was upregulated at the injury site. Depending on the type of edema, AQP4 upregulation can be either protective or deleterious. In vasogenic brain edema, increased levels of AQP4 facilitate the removal of excess of fluid. Contrary, in cytotoxic brain edema, AQP4 upregulation accompanies with enlarged brain water accumulation.

The finding that histamine has a negative effect on cellular AQP4 expression is contradictious to literature where the levels of AQP4 are increased following TBI. Nevertheless, complex pathways are activated after TBI, which might have an opposite effect on AQP4 and the course of brain edema. However, the histamine-mediated loss of functional water channels impairs the rate of water flow in the brain. This may have serious consequences for the course of TBI-associated brain edema. Declined bidirectional water flow may have a beneficial effect on the development of cytotoxic edema, because the water transport through AQP4 is highly restricted. Conversely during vasogenic edema, histamine may have a detrimental effect because the clearance of accumulated water is as well reduced. Dependent on the type of brain edema, the use of histamine antagonists could have a huge potential.

4.3 Future perspectives

The ability to identify accurate AQP4 supramolecular structures and dynamics permits the study of molecular determinants for OAP assembly. Further investigations may as well focus on AQP4-M1 and AQP4-M23 co-expression experiments because the interplay between both can also affect OAP size (14).

In the present study two different techniques were used to study the behavior of AQP4 isoforms. Both techniques have intrinsic characteristics, which might be responsible for alterations in the calculated diffusion coefficient. FRAP can be biased because fast moving particles of the population influence the recovery of the fluorescent signal and consequently the diffusion coefficient can be overestimated. In SPT, slow moving particles are more easily tracked than fast moving particles. Furthermore, there is a fundamental difference in approach between both techniques. FRAP measures the time required for a particle to overcome a fixed distance, whereas SPT measures the distance travelled by the protein during a well-defined time frame. The minimal fixed distance in FRAP is easily an order of magnitude larger than the minimal displacement that can be detected by SPT due to the diffraction limit (68). Therefore, calculation of the diffusion coefficient of AQP4-M1 using SPT might be desirable for future investigations because it would allow a better comparison between both isoforms. SPT was carried out with primary antibodies labeled with Alexa Fluor® 488. Future research using SPT might be improved by using primary antibodies conjugated with semiconductor nanocrytals, known as quantum dots (QDs). QDs show several advantages over most organic fluorophore dyes. QDs have a very broad absorption pattern, which permits efficiently excitation far from their emission spectra to minimize background scattering. Besides, QDs generate nearly Gaussian emission peaks where organic dyes display shoulders in their emission spectra. This allows efficient co-tracking of both AQP4-M1 and AQP4-M23 together with one or more regulatory proteins. Moreover, QDs have far greater quantum yields and photostability than organic dyes at similar wavelengths. This allows QD-labeled particles to be tracked for longer periods of time. QDs show only few disadvantages, being relatively large with a typical size ranging from 10-30 nm and their blinking behavior where dark periods of no emission interrupt periods of fluorescence (69).

Although SPT has proven to be a powerful technique, imaging the temporal and spatial distribution of OAPs over the cell surface might be useful. TICS can measure the number density and aggregation of fluorescent labeled molecules, their diffusion coefficient and flow speed. In this way, both aggregation and diffusion can be studied together (42). Furthermore, this can be combined with the use of genetically encoding fluorescent proteins, which are ligated in the AQP4 sequence. Previously, it was shown that inserting of GFP in the second extracellular loop did not interfere with protein tracking of function (10). The advantages of this approach include that no labeling or fixation is necessary to study AQP4.

4.4 Microfluorimetric *in vitro* model for assessment of OAP alteration

In present study, microfluorimetric measurements were performed to identify OAP alternation after histamine challenge. After implementation of other microfluorimetric techniques previously mentioned, including SPT for AQP4-M1 and TICS, in combination with current techniques an *in vitro* model for assessment of OAP alternation can be generated. Because other neuronal mediators, which are released following TBI, might impact on AQP4 as well, this *in vitro* model can elucidate new relations between both.

Addition of patient material (e.g. CSF) which contains these neuronal mediators can be added in this model. Together with proteomic analyses of the composition of the patient material, this approach could shed light on other neuronal mediators which influence AQP4 supramolecular assembly as well. Furthermore, together with functional tests, this model can in future be applied for drug screening purposes where potent and non-potent AQP4 modulators can be discriminated.

Chapter 5: Conclusion

TBI is a leading cause of death and disability worldwide, where the complication of brain edema is a key contributor to the TBI-associated morbidity and mortality. Nevertheless, the cellular and molecular mechanisms contributing to the development or resolution of TBI-associated brain edema are poorly understood. A key role for AQP4 has been suggested. AQP4 is a most prominent water channel protein of the CNS, where its localized distribution across blood-brain interfaces suggests its importance in maintaining the water homeostasis in the brain. OAP assembly is crucial in regulating the bidirectional water flow. The release of neuronal mediators after TBI may contribute to the development of brain edema by exerting unfavorable effects on OAPs. In present study, the effect of the neuronal mediator histamine on AQP4 supramolecular organization in OAPs was investigated. In the first part, the feasibility of microfluorimetric techniques in investigating the higher-order organization and dynamic behavior of AQP4 in the cell membrane was explored. In order to address questions about the regulation of OAP dynamics and membrane organization, the clustering in OAPs should be accurately determined. ICS was shown to be convenient in defining the static aggregation of AQP4 in the cell membrane. Furthermore, FRAP and SPT were valuable for AQP4-M1 and AQP4-M23, respectively, to study diffusion in the membrane. In the second part, it was hypothesized that the astrocytic higher-order structure of AQP4 was disrupted after exposure to histamine. Immunofluorescence showed that histamine challenge induced a translocation of AQP4 from the cell membrane to the cytoplasm which as accompanied with intracellular vesicles containing AQP4. This internalization was most pronounced in AQP4-M23 overexpressing lines. Nevertheless, the source of these vesicles remains speculative. Colocalization with the late endosomal marker Rab7a was questionable and the vesicles might represent recycling endosomes as well. ICS analyses showed that the brightness of AQP4-M1 increased after 15 minutes of 10 mM histamine exposure, proposing that an endocytosis related process was ongoing. Furthermore, the degree of aggregation of AQP4-M23 was significantly decreased after histamine challenge. Moreover, FRAP and SPT analyses were in agreement with the ICS results because AQP4 diffusion significantly increased. These findings are in accordance with the results in Nuydens et al (unpublished results), where histamine also impairs the hypotonicity induced cell swelling response and worsened ICP in a rat model. The loss of functional water channels compromised the rate of water flow in the brain. This may have serious consequences for the course of TBI-associated brain edema. In vasogenic edema, histamine may have a detrimental effect because the clearance of accumulated water will be reduced. Maintaining AQP-4 functionality may thus form an interesting tool to remove excess water from the brain after traumatic brain injury. The use of histamine antagonists could have a potential as a therapy for brain edema. Furthermore, microfluorimetric measurements proved to be a significant tool to visualize AQP4 molecules and their supramolecular organization in OAPs in living cells. These biophysical methods allow the study of molecular determinants of AQP4 assembly. Combination with other *in vitro* tests, for instance cell swelling assays, would allow the identification of other neuronal mediators which exert an effect on AQP4 mediated water flow or could have its application in drug screening purposes.

References

1. Helmy A., De Simoni M. G., Guilfoyle M. R., Carpenter K. L., Hutchinson P. J. Cytokines and innate inflammation in the pathogenesis of human traumatic brain injury. Prog Neurobiol. 2011 Nov;95(3):352-72.
2. Shin J. A., Choi J. H., Choi Y. H., Park E. M. Conserved aquaporin 4 levels associated with reduction of brain edema are mediated by estrogen in the ischemic brain after experimental stroke. Biochim Biophys Acta. 2011 Sep;1812(9):1154-63.
3. Benga G. Water channel proteins (later called aquaporins) and relatives: past, present, and future. IUBMB Life. 2009 Feb;61(2):112-33.
4. Ishibashi K., Hara S., Kondo S. Aquaporin water channels in mammals. Clin Exp Nephrol. 2009 Apr;13(2):107-17.
5. Hachez C., Chaumont F. Aquaporins: a family of highly regulated multifunctional channels. Adv Exp Med Biol. 2010;679:1-17.
6. Iacovetta C., Rudloff E., Kirby R. The role of aquaporin 4 in the brain. Vet Clin Pathol. 2012 Jan 17.
7. De Jongh R., Nuydens R., Smets A., Vissers K., Meert T. Aquaporin-4 in the brain: A review. Current Topics in Pharmacology. 2008;12(2):62.
8. Amiry-Moghaddam M., Frydenlund D. S., Ottersen O. P. Anchoring of aquaporin-4 in brain: molecular mechanisms and implications for the physiology and pathophysiology of water transport. Neuroscience. 2004;129(4):999-1010.
9. Suzuki H., Nishikawa K., Hiroaki Y., Fujiyoshi Y. Formation of aquaporin-4 arrays is inhibited by palmitoylation of N-terminal cysteine residues. Biochim Biophys Acta. 2008 Apr;1778(4):1181-9.
10. Tajima M., Crane J. M., Verkman A. S. Aquaporin-4 (AQP4) associations and array dynamics probed by photobleaching and single-molecule analysis of green fluorescent protein-AQP4 chimeras. J Biol Chem. 2010 Mar 12;285(11):8163-70.
11. Silberstein C., Bouley R., Huang Y., Fang P., Pastor-Soler N., Brown D., et al. Membrane organization and function of M1 and M23 isoforms of aquaporin-4 in epithelial cells. Am J Physiol Renal Physiol. 2004 Sep;287(3):F501-11.
12. Rossi A., Crane J. M., Verkman A. S. Aquaporin-4 Mz isoform: brain expression, supramolecular assembly and neuromyelitis optica antibody binding. Glia. 2011 Jul;59(7):1056-63.
13. Ho J. D., Yeh R., Sandstrom A., Chorny I., Harries W. E., Robbins R. A., et al. Crystal structure of human aquaporin 4 at 1.8 A and its mechanism of conductance. Proc Natl Acad Sci U S A. 2009 May 5;106(18):7437-42.
14. Crane J. M., Bennett J. L., Verkman A. S. Live cell analysis of aquaporin-4 m1/m23 interactions and regulated orthogonal array assembly in glial cells. J Biol Chem. 2009 Dec 18;284(51):35850-60.
15. Zelenina M. Regulation of brain aquaporins. Neurochem Int. 2010 Nov;57(4):468-88.
16. Fenton R. A., Moeller H. B., Zelenina M., Snaebjornsson M. T., Holen T., MacAulay N. Differential water permeability and regulation of three aquaporin 4 isoforms. Cell Mol Life Sci. 2010 Mar;67(5):829-40.
17. Crane J. M., Van Hoek A. N., Skach W. R., Verkman A. S. Aquaporin-4 dynamics in orthogonal arrays in live cells visualized by quantum dot single particle tracking. Mol Biol Cell. 2008 Aug;19(8):3369-78.

18. Zelenina M., Zelenin S., Bondar A. A., Brismar H., Aperia A. Water permeability of aquaporin-4 is decreased by protein kinase C and dopamine. Am J Physiol Renal Physiol. 2002 Aug;283(2):F309-18.

19. McAllister T. W. Neurobiological consequences of traumatic brain injury. Dialogues Clin Neurosci. 2011;13(3):287-300.

20. Aarabi B., Simard J. M. Traumatic brain injury. Curr Opin Crit Care. 2009 Dec;15(6):548-53.

21. Nag S., Manias J. L., Stewart D. J. Pathology and new players in the pathogenesis of brain edema. Acta Neuropathol. 2009 Aug;118(2):197-217.

22. Papadopoulos M. C., Verkman A. S. Aquaporin-4 and brain edema. Pediatr Nephrol. 2007 Jun;22(6):778-84.

23. Zador Z., Stiver S., Wang V., Manley G. T. Role of aquaporin-4 in cerebral edema and stroke. Handb Exp Pharmacol. 2009(190):159-70.

24. Xu M., Su W., Xu Q. P. Aquaporin-4 and traumatic brain edema. Chin J Traumatol. 2010 Apr 1;13(2):103-10.

25. Manley G. T., Fujimura M., Ma T. H., Noshita N., Filiz F., Bollen A. W., et al. Aquaporin-4 deletion in mice reduces brain edema after acute water intoxication and ischemic stroke. Nat Med. [Article]. 2000 Feb;6(2):159-63.

26. Papadopoulos M. C., Verkman A. S. Aquaporin-4 gene disruption in mice reduces brain swelling and mortality in pneumococcal meningitis. J Biol Chem. 2005 Apr 8;280(14):13906-12.

27. Manley G. T., Binder D. K., Papadopoulos M. C., Verkman A. S. New insights into water transport and edema in the central nervous system from phenotype analysis of aquaporin-4 null mice. Neuroscience. 2004;129(4):983-91.

28. Papadopoulos M. C., Manley G. T., Krishna S., Verkman A. S. Aquaporin-4 facilitates reabsorption of excess fluid in vasogenic brain edema. FASEB J. 2004 Aug;18(11):1291-3.

29. Vajda Z., Pedersen M., Fuchtbauer E. M., Wertz K., Stodkilde-Jorgensen H., Sulyok E., et al. Delayed onset of brain edema and mislocalization of aquaporin-4 in dystrophin-null transgenic mice. Proc Natl Acad Sci U S A. 2002 Oct 1;99(20):13131-6.

30. Nicchia G. P., Mastrototaro M., Rossi A., Pisani F., Tortorella C., Ruggieri M., et al. Aquaporin-4 orthogonal arrays of particles are the target for neuromyelitis optica autoantibodies. Glia. 2009 Oct;57(13):1363-73.

31. Lozada A., Maegele M., Stark H., Neugebauer E. M., Panula P. Traumatic brain injury results in mast cell increase and changes in regulation of central histamine receptors. Neuropathol Appl Neurobiol. 2005 Apr;31(2):150-62.

32. Shimada R., Nakao K., Furutani R., Kibayashi K. A rat model of changes in dural mast cells and brain histamine receptor H3 expression following traumatic brain injury. J Clin Neurosci. 2012 Mar;19(3):447-51.

33. Ferstl R., Akdis C. A., O'Mahony L. Histamine regulation of innate and adaptive immunity. Front Biosci. 2012;17:40-53.

34. Haas H. L., Sergeeva O. A., Selbach O. Histamine in the nervous system. Physiol Rev. 2008 Jul;88(3):1183-241.

35. Carmosino M., Procino G., Tamma G., Mannucci R., Svelto M., Valenti G. Trafficking and phosphorylation dynamics of AQP4 in histamine-treated human gastric cells. Biol Cell. 2007 Jan;99(1):25-36.

36. Carmosino M., Procino G., Nicchia G. P., Mannucci R., Verbavatz J. M., Gobin R., et al. Histamine treatment induces rearrangements of orthogonal arrays of particles (OAPs) in human AQP4-expressing gastric cells. J Cell Biol. 2001 Sep 17;154(6):1235-43.

37. Crane J. M., Verkman A. S. Determinants of aquaporin-4 assembly in orthogonal arrays revealed by live-cell single-molecule fluorescence imaging. J Cell Sci. 2009 Mar 15;122(Pt 6):813-21.

38. Sorbo J. G., Moe S. E., Ottersen O. P., Holen T. The molecular composition of square arrays. Biochemistry. 2008 Feb 26;47(8):2631-7.

39. Crane J. M., Tajima M., Verkman A. S. Live-cell imaging of aquaporin-4 diffusion and interactions in orthogonal arrays of particles. Neuroscience. 2010 Jul 28;168(4):892-902.

40. Owen D. M., Williamson D., Rentero C., Gaus K. Quantitative microscopy: protein dynamics and membrane organisation. Traffic. 2009 Aug;10(8):962-71.

41. Al-Soufi W., Reija B., Felekyan S., Seidel C. A., Novo M. Dynamics of supramolecular association monitored by fluorescence correlation spectroscopy. Chemphyschem. 2008 Sep 15;9(13):1819-27.

42. Kolin D. L., Wiseman P. W. Advances in image correlation spectroscopy: measuring number densities, aggregation states, and dynamics of fluorescently labeled macromolecules in cells. Cell Biochem Biophys. 2007;49(3):141-64.

43. Petersen N. O., Hoddelius P. L., Wiseman P. W., Seger O., Magnusson K. E. Quantitation of membrane receptor distributions by image correlation spectroscopy: concept and application. Biophys J. 1993 Sep;65(3):1135-46.

44. Srivastava Mamta, Petersen Nils O. Image cross-correlation spectroscopy: A new experimental biophysical approach to measurement of slow diffusion of fluorescent molecules. Methods in Cell Science. 1996;18(1):47-54.

45. Mattheyses A. L., Simon S. M., Rappoport J. Z. Imaging with total internal reflection fluorescence microscopy for the cell biologist. J Cell Sci. [Article]. 2010 Nov;123(21):3621-8.

46. Levi V., Gratton E. Exploring dynamics in living cells by tracking single particles. Cell Biochem Biophys. 2007;48(1):1-15.

47. Saito M., Tanaka H., Sasaki M., Kurose H., Nakahata N. Involvement of aquaporin in thromboxane A2 receptor-mediated, G 12/13/RhoA/NHE-sensitive cell swelling in 1321N1 human astrocytoma cells. Cell Signal. 2010 Jan;22(1):41-6.

48. Henis Yoav I., Rotblat Barak, Kloog Yoel. FRAP beam-size analysis to measure palmitoylation-dependent membrane association dynamics and microdomain partitioning of Ras proteins. Methods. 2006;40(2):183-90.

49. Wiseman P. W., Petersen N. O. Image correlation spectroscopy. II. Optimization for ultrasensitive detection of preexisting platelet-derived growth factor-beta receptor oligomers on intact cells. Biophys J. 1999 Feb;76(2):963-77.

50. Yang B., Brown D., Verkman A. S. The mercurial insensitive water channel (AQP-4) forms orthogonal arrays in stably transfected Chinese hamster ovary cells. J Biol Chem. 1996 Mar 1;271(9):4577-80.

51. Rash J. E., Yasumura T., Hudson C. S., Agre P., Nielsen S. Direct immunogold labeling of aquaporin-4 in square arrays of astrocyte and ependymocyte plasma membranes in rat brain and spinal cord. Proc Natl Acad Sci U S A. 1998 Sep 29;95(20):11981-6.

52. Rossi A., Pisani F., Nicchia G. P., Svelto M., Frigeri A. Evidences for a leaky scanning mechanism for the synthesis of the shorter M23 protein isoform of aquaporin-4: implication in orthogonal array formation and neuromyelitis optica antibody interaction. J Biol Chem. 2010 Feb 12;285(7):4562-9.

53. Nuydens R., De Jongh R., Nevelsteen J., Smets A. , Van Deuren B. , Meert T. Aquaporin-4 mediated waterfluxes are compromised by histamine in astrocytoma cells in vitro and in rat brain in vivo. 2010.

54. Mertens S. The study of AQP4-mediated cell volume regulation in astrocytoma cells. Diepenbeek: Hasselt University; 2007.

55. Ullrich O., Reinsch S., Urbe S., Zerial M., Parton R. G. Rab11 regulates recycling through the pericentriolar recycling endosome. J Cell Biol. 1996 Nov;135(4):913-24.

56. Self T. J., Oakley S. M., Hill S. J. Clathrin-independent internalization of the human histamine H1-receptor in CHO-K1 cells. Br J Pharmacol. 2005 Oct;146(4):612-24.

57. Laboisse C. L., Augeron C., Couturier-Turpin M. H., Gespach C., Cheret A. M., Potet F. Characterization of a newly established human gastric cancer cell line HGT-1 bearing histamine H2-receptors. Cancer Res. 1982 Apr;42(4):1541-8.

58. Han Z., Wax M. B., Patil R. V. Regulation of aquaporin-4 water channels by phorbol ester-dependent protein phosphorylation. J Biol Chem. 1998 Mar 13;273(11):6001-4.

59. McCoy E. S., Haas B. R., Sontheimer H. Water permeability through aquaporin-4 is regulated by protein kinase C and becomes rate-limiting for glioma invasion. Neuroscience. 2010 Jul 28;168(4):971-81.

60. Karasu A., Aras Y., Sabanci P. A., Saglam G., Izgi N., Biltekin B., et al. The effects of protein kinase C activator phorbol dibutyrate on traumatic brain edema and aquaporin-4 expression. Ulus Travma Acil Cerrahi Derg. 2010 Sep;16(5):390-4.

61. Fazzina G., Amorini A. M., Marmarou C. R., Fukui S., Okuno K., Dunbar J. G., et al. The protein kinase C activator phorbol myristate acetate decreases brain edema by aquaporin 4 downregulation after middle cerebral artery occlusion in the rat. J Neurotrauma. 2010 Feb;27(2):453-61.

62. Ke C., Poon W. S., Ng H. K., Pang J. C., Chan Y. Heterogeneous responses of aquaporin-4 in oedema formation in a replicated severe traumatic brain injury model in rats. Neurosci Lett. 2001 Mar 23;301(1):21-4.

63. Zhao J., Moore A. N., Clifton G. L., Dash P. K. Sulforaphane enhances aquaporin-4 expression and decreases cerebral edema following traumatic brain injury. J Neurosci Res. 2005 Nov 15;82(4):499-506.

64. Sun M. C., Honey C. R., Berk C., Wong N. L., Tsui J. K. Regulation of aquaporin-4 in a traumatic brain injury model in rats. J Neurosurg. 2003 Mar;98(3):565-9.

65. Neal C. J., Lee E. Y., Gyorgy A., Ecklund J. M., Agoston D. V., Ling G. S. Effect of penetrating brain injury on aquaporin-4 expression using a rat model. J Neurotrauma. 2007 Oct;24(10):1609-17.

66. Saadoun S., Papadopoulos M. C., Krishna S. Water transport becomes uncoupled from K+ siphoning in brain contusion, bacterial meningitis, and brain tumours: immunohistochemical case review. J Clin Pathol. 2003 Dec;56(12):972-5.

67. Hu H., Yao H. T., Zhang W. P., Zhang L., Ding W., Zhang S. H., et al. Increased expression of aquaporin-4 in human traumatic brain injury and brain tumors. J Zhejiang Univ Sci B. 2005 Jan;6(1):33-7.

68. Smisdom N. The dynamic behavior of the glycine receptor in the plasma membrane. Diepenbeek: University of Hasselt; 2011.

69. Barroso M. M. Quantum dots in cell biology. J Histochem Cytochem. 2011 Mar;59(3):237-51.

Auteursrechtelijke overeenkomst

Ik/wij verlenen het wereldwijde auteursrecht voor de ingediende eindverhandeling:
The influence of aquaporin-4 isoform interaction on supramolecular water channel assembly in astrocytoma cells

Richting: **master in de biomedische wetenschappen-klinische moleculaire wetenschappen**
Jaar: **2012**

in alle mogelijke mediaformaten, - bestaande en in de toekomst te ontwikkelen - , aan de Universiteit Hasselt.

Niet tegenstaand deze toekenning van het auteursrecht aan de Universiteit Hasselt behoud ik als auteur het recht om de eindverhandeling, - in zijn geheel of gedeeltelijk -, vrij te reproduceren, (her)publiceren of distribueren zonder de toelating te moeten verkrijgen van de Universiteit Hasselt.

Ik bevestig dat de eindverhandeling mijn origineel werk is, en dat ik het recht heb om de rechten te verlenen die in deze overeenkomst worden beschreven. Ik verklaar tevens dat de eindverhandeling, naar mijn weten, het auteursrecht van anderen niet overtreedt.

Ik verklaar tevens dat ik voor het materiaal in de eindverhandeling dat beschermd wordt door het auteursrecht, de nodige toelatingen heb verkregen zodat ik deze ook aan de Universiteit Hasselt kan overdragen en dat dit duidelijk in de tekst en inhoud van de eindverhandeling werd genotificeerd.

Universiteit Hasselt zal mij als auteur(s) van de eindverhandeling identificeren en zal geen wijzigingen aanbrengen aan de eindverhandeling, uitgezonderd deze toegelaten door deze overeenkomst.

Voor akkoord,

Deville, Sarah

Datum: **11/06/2012**